7630 *J. Phys. Chem. A* **2009,** *113,* 7630–7646

The Cl + H_2 → HCl + H Reaction Induced by IR + UV Irradiation of Cl_2 in Solid *para*-H_2: Quantum Model Simulation†

M. V. Korolkov,[‡,§] J. Manz,[*,‡] and A. Schild[‡]

Institut für Chemie and Biochemie, Freie Universität Berlin, Takustraβe 3, 14195 Berlin, Germany, and Institute of Physics, National Academy of Sciences of Belarus, Minsk, Belarus

Received: January 13, 2009; Revised Manuscript Received: March 4, 2009

Recent experimental investigations by the group of D. T. Anderson (Kettwich, S. C.; Raston, P. L.; Anderson, D. T. *J. Phys. Chem. A* **2009**, *113*, DOI 10.1021/jp811206a) show that the reaction Cl + H_2 → HCl + H in the *para*-H_2 crystal can be induced by infrared (IR) + ultraviolet (UV) coirradiations causing vibrational pre-excitation of the molecular reactant, $H_2(v=1)$, and generation of the atomic reactant, $Cl(^2P_{3/2})$, by near-resonant photodissociation of a matrix-isolated Cl_2 molecule in the C $^1\Pi_u$ state, respectively. The corresponding reaction probability $P_{v=1}$ for the reactants Cl + $H_2(v=1)$ is ~0.15; this is ~25 times larger than $P_{v=0}$ for Cl + $H_2(v=0)$ (as initiated by pure UV irradiation). We present a simple three-step quantum model which accounts for some important parts of the experimental results and allows predictions for other scenarios, for example, UV photodissociation of the Cl_2 molecule by a laser pulse. The first step, vibrational pre-excitation of H_2, yields the molecular initial state which is described using the Einstein model of the *para*-H_2 crystal. The second step, photodissociation of Cl_2, generates the $Cl(^2P_{3/2})$ atom approaching $H_2(v=1)$. In the third step, Cl reacts with $H_2(v=1)$ much more efficiently than with $H_2(v=0)$ close to threshold. The ultrashort time domains (~100 fs) of steps 2 plus 3 support one- and then two-dimensional models of photodissociation of Cl_2 by short laser pulses and of the subsequent reaction of the system Cl−H−H embedded in frozen environments. The widths of the corresponding wave function describing the translational motion of the reactants is revealed as a significant parameter which is determined not only by the duration of the laser pulse but, even more importantly, by the width of the Gaussian-type distribution of the center of mass of the H_2 molecule in its Einstein cell. As a consequence, the resulting P_v are quite robust versus variations of the UV pulse durations, allowing extrapolations to continuous wave irradiation. Quantum dynamics simulations of the reaction reveal that the experimental results are due to energetic and dynamical effects.

I. Introduction

The purpose of this paper is to present the first quantum model investigation of a state-selective elementary chemical reaction in a quantum crystal. Specifically, we consider the reaction

$$Cl(^2P_{3/2}) + H_2(v = 1) \rightarrow HCl + H \tag{1}$$

in solid *para*-H_2 and compare it with the dominantly elastic collision

$$\begin{aligned} Cl(P_{3/2}) + H_2(v = 0) &\rightarrow Cl + H_2(v' = 0) \\ &\nrightarrow HCl + H \end{aligned} \tag{2}$$

for the same, rather low value of translational energy E_{trans} close to threshold and also with the reaction

$$Cl(^2P_{3/2}) + H_2(v = 0) \rightarrow HCl + H \tag{3}$$

at larger translational energy $\tilde{E}_{trans}$ such that reactions 1 and 3 have the same total (= vibrational + translational) energies

$$E_{tot} = E_{H_2,v=1} + E_{trans} = E_{H_2,\tilde{v}=0} + \tilde{E}_{trans} \tag{4}$$

Note the different notations without and with primes (′), which are used in eqs 1−4 and below in order to specify the properties of the Cl−H−H system (e.g., the vibrational quantum numbers v versus v' or the translational energies E_{trans} versus E'_{trans}) before and after the collision or reaction, respectively. In contrast, we use the tilde (~) in order to distinguish different partitionings of the same total energy into vibrational plus translational energies of the reactants; compare eq 4.

Our investigation is motivated by recent corresponding experimental studies by the group of D. T. Anderson,[1] which prepared the reactants with selective vibrational states $v = 0$ or 1 and with specific, rather low mean values of the translational energy E_{trans}, different from their approach[2,3] (see below for the details). In general, the investigation should provide several extensions of previous studies, for example, from nonreactive molecular processes in quantum crystals (see, for example, refs 4 and 5) to reactive ones (compare with ref 6), from photoinduced reactions in rare gas matrixes (see, for example, refs 7−12) to quantum crystals, or from studies of reaction 1 in the gas (see, for example, refs 13−21) to the condensed phase. Since reaction 1 is actually induced by specific irradiation of matrix-

---

† Part of the "Robert Benny Gerber Festschrift".

* To whom correspondence should be addressed. E-mail: jmanz@chemie.fu-berlin.de.

‡ Freie Universität Berlin.

§ National Academy of Sciences of Belarus.

10.1021/jp9003455 CCC: $40.75

isolated Cl_2 molecules embedded in *para*-H_2 crystals (again, see below for the details), our investigation may also be considered as a prototype study of photoinduced quantum solvent−solute reactions.

The recent[1] and previous[2,3] experimental studies of reactions 1 and 2 in solid *para*-H_2 by the group of D. T. Anderson use two different approaches to initiate the reaction. The original one, referred to as IR, employs a sequence of ultraviolet plus infrared irradiations, where the first (UV) one generates $Cl(^2P_{3/2})$ atoms isolated in *para*-H_2 cages by near-resonant photodissociation of matrix-isolated Cl_2 molecules in the C $^1\Pi_u$ state, followed by the second (IR) one which prepares a "vibron" of delocalized reactant molecules $H_2(v)$ in the vibrationally excited state $v = 1$.[2,3] In contrast, the recent approach, called "IR + UV", employs IR + UV coirradiations, thus causing IR vibrational pre-excitation of the "vibron" $H_2(v{=}1)$ and simultaneous UV photodissociation of Cl_2.[1] The measured reaction probability for reaction 1 starting from the vibrationally pre-excited $H_2(v{=}1)$ is $P_{v=1} \approx 0.15$. This is about 25 times larger than $P_{v=0} \approx 0.006$ for the corresponding reactants $Cl + H_2(v{=}0)$. The latter is induced by pure near-resonant UV photodissociation of the $Cl_2(C\ ^1\Pi_u)$ molecule, referred to as the "only UV" experiment. For the present purpose, we employ the new IR + UV approach because by a working hypothesis, it supports ultrafast direct reaction of the nascent Cl atom with the neighboring vibrationally pre-excited $H_2(v{=}1)$ molecule. This mechanism lends itself to a rather simple three-step model for the quantum simulations in convenient time domains of few hundred femtoseconds (1 fs $= 10^{-15}$ s), that is, the reaction occurs while the environment (i.e., all other *para*-H_2 molecules) may be considered approximately as frozen. The corresponding comparison of the IR + UV and the "only UV" mechanisms should reveal important aspects of the reaction in the quantum solid, and the results should serve as a reference for more sophisticated quantum simulations. In contrast, quantum simulation of the alternative "IR" approach would be much more difficult, for example, it would call for adequate description of the trapping of the photodissociated Cl atoms in *para*-H_2 cages, which relax on much longer time scales before IR excitation of the vibron $H_2(v{=}1)$ and subsequent reaction.

The paper is organized as follows. Section II derives the three-step model, literally step-by-step. Sections III and IV have the results and discussions and the conclusions and an outlook, respectively.

II. A Three-Step Model for Quantum Dynamics Simulations of the Cl + H_2 Reaction in a *para*-H_2 Crystal Induced by IR + UV versus Only UV Irradiation

A. Model Assumptions. Our three-step model for the Cl + H_2 reaction in the *para*-H_2 crystal is based on several working hypotheses and approximations which are explained below; see items (i)−(ix). Note that for convenience, all of the relevant properties and parameters of the system as well as the results will be expressed using the units of a_0 for lengths, fs for times, eV for energies, and u for atomic mass units. The quantum dynamics simulations are carried out, nevertheless, using atomic units, that is, a_0, $\hbar/E_h$, E_h, and m_e, respectively. The resulting wave functions are written with the general notation $\Psi_{\text{parameters}}(\text{coordinates,time})$, where the set of parameters quantify specific effects of the three-step model.

(i) First, for step 1 of the three-step model, we assume that the vibrationally excited educt molecule $H_2(v{=}1)$ of reaction 1 is prepared readily for reaction, without considering the microscopic details of the experimental IR excitation. The latter generates a "vibron" of vibrational excitations ($v = 1$) which is delocalized over several *para*-hydrogen molecules.[1] In contrast, we consider a simplified scenario where the vibrational excitation is localized in a single $H_2(v{=}1)$ molecule. Moreover, we assume that this $H_2(v{=}1)$ molecule is embedded in the cage surrounding the matrix-isolated Cl_2 precursor molecule, such that the direction of the Cl_2 bond points to the pre-excited $H_2(\nu)$. As a consequence, we anticipate that the resulting reaction probability $P_{v=1}$ of the present model reaction 1 is an upper limit to the experimental one because in our scenario, the nascent Cl atom is directed to the single, neighboring excited molecule $H_2(v{=}1)$, instead of the realistic distribution of presumably less efficient attacks to the delocalized vibron.

(ii) Second, the reactant molecule $H_2(\nu)$ is described using the Einstein model of the *para*-H_2 crystal, adapted from ref 22. Essentially, it describes the motion of the center of mass (c.o.m.) of the $H_2(\nu)$ molecule embedded in an Einstein cell of the *para*-H_2 crystal. The model accounts for the characteristic structural and energetic properties of solid *para*-H_2, such as the nearest neighbor distance (compare the theoretical result $R_0 = 7.29\ a_0$, which will be employed in the subsequent application, with the experimental value $R_0 = 7.16\ a_0$) or the sublimation energy including significant contributions of zero-point energies, as well as isotope effects (cf. ref 23). In particular, it describes the pair distribution function for the nearest neighbors (cf. ref 24), with Gaussian-type shape and rather broad widths, which is typical for the quantum solid (full width at half-maximum fwhm $= 2.01\ a_0 = 2(\ln 2)^{1/2}\cdot\Delta R_{H_2}$, where $\Delta R_{H_2} = 1.21\ a_0$).[22] The effective potential for the motion of the center of mass (c.o.m.) of the H_2 molecule is approximately harmonic, within the widths ΔR_{H_2}.[22]

(iii) Third, we assume that the Cl_2 molecule can be described by a model similar to the Einstein model for the H_2 molecule,[22] that is, it is isolated in an Einstein-type cage with similar properties. In particular, the effective potential for the motion of the c.o.m. of the Cl_2 molecule is again approximately harmonic, within the domain of the corresponding widths ΔR_{Cl_2}, with a similar force constant as that for the Einstein model of H_2. The widths parameters ΔR_{Cl_2} and ΔR_{H_2} can then be related to each other approximately, using the ubiquitious model of the harmonic oscillator

$$\begin{aligned}\Delta R_{Cl_2} &\approx \left(\frac{m_H}{m_{Cl}}\right)^{1/2}\Delta R_{H_2} \\ &\approx 0.170\Delta R_{H_2}\end{aligned} \tag{5}$$

Here and below, we use the masses $m_H = 1.0079$ u and $m_{Cl} = 34.968852$ u. By definition, the mean value of the center of mass of the Cl_2 embedded in the *para*-H_2 crystal is at the origin. We assume that the distance to the mean value of the c.o.m. of the molecular reactant $H_2(v)$ is again $R_0 = 7.29\ a_0$.

(iv) Fourth, for step 2 of the three-step model, we consider symmetrical photodissociation via near-resonant UV excitation of the state $Cl_2(C\ ^1\Pi_u)$ by means of short laser pulses; the results will also be extrapolated to the effects of continuous wave excitations. The laser−molecule interaction is described using the semiclassical dipole approximation. Essentially, in the molecular (Cl_2) frame, the laser produces two $Cl(^2P_{3/2})$ atoms with coordinates q_1 and $q_{-1} = -q_1$ moving toward opposite directions, with opposite momenta $\hbar k$ and $-\hbar k$, that is, the bond distance is $r = 2q_1$; compare Figure 1. Modifications due to the motion of the c.o.m. of

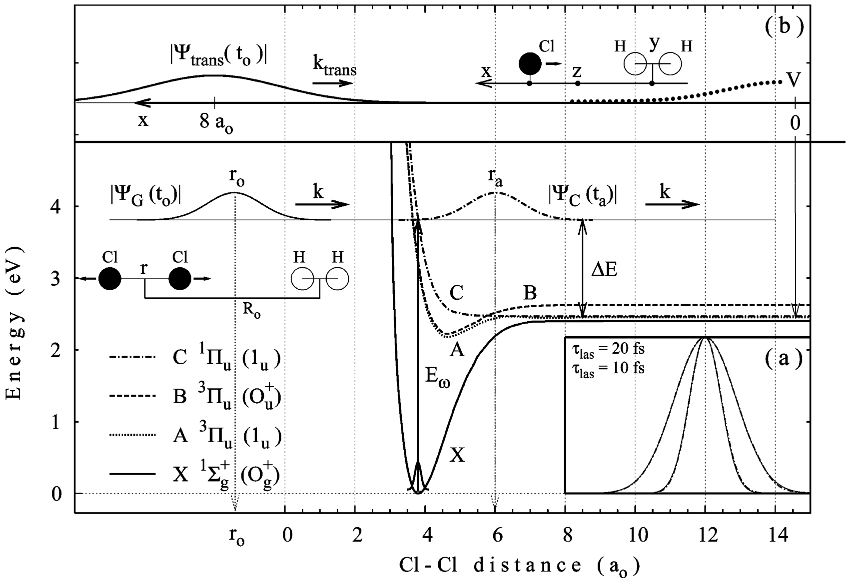

Figure 1. UV photodisscociation of the Cl_2 molecule embedded in a *para*-H_2 crystal and subsequent approach of one of the Cl atoms to the neighboring H_2 molecule. The initial ($t = 0$) wave function $\chi_{X,v=0}(r)$ representing Cl_2 in the electronic ground state X and vibrational ground state $v = 0$ is shown embedded in the potential energy curve $V_X(r)$ versus Cl−Cl bond distance r. The baseline of $\chi_{v=0}(r)$ indicates its zero-point energy $E_{Cl_2,v=0}$. Franck−Condon-type "vertical" photoexcitation by a UV laser pulse with photon energy $E_\omega = \hbar\omega = 3.782$ eV (adapted from ref 1), the Gaussian shape, and the duration τ induce a transition to the dissociative electronic excited C state, as illustrated by the vertical arrow from $E_{X,v=0}$ to the potential curve $V_C(r)$. The various potential curves labeled X, A, B, and C are adapted from the ab initio calculations of refs 32 and 33 for the gas phase, as approximations to the crystal which are valid in the domain of small bond distances, $r < r_a \approx 6$ a_0. For larger values of r, significant interactions of the dissociated Cl atoms with the neighboring H_2 molecules cause deviations from the gaseous reference, as indicated by the dotted line labeled "V" in panel (b). The photodissociated wavepacket $\Psi_C(t_a)$ at time t_a (= 67 fs) when it is centered at r_a for the case of the laser duration $\tau = 20$ fs is illustrated by its absolute value superimposed on the horizontal line which represents an artificial constant potential $V_G = E_{Cl_2,v=0} + E_\omega$, with corresponding momentum $k(\omega)$, eqs 20−22. The inset in (a) shows almost perfect agreement of the (absolute values of) wave functions $\Psi_C(t_a)$ (dash−dotted lines) centered at r_a for laser durations $\tau = 20$ and 10 fs and corresponding Gaussian wave functions $\Psi_G(t_a)$ (continuous lines), with width parameter $\Delta r(\tau)$ increasing with laser duration τ and moving along r with the same momentum $k(\omega)$. Also shown is the Gaussian wave function $\Psi_G(t_0)$ at time t_0 ($t_a - t_0 = 100$ fs) when it is centered at $r_0 = -1.42$ a_0, back-propagated from $\Psi_G(t_a)$ on V_G, eq 25. The $\Psi_G(t_0)$ is used to construct the initial wave function $\Psi_{trans}(t_0)$ moving along the coordinate x (= distance between the Cl atom and the center fo mass of the H_2 molecule) for the translational motion betwen Cl and H_2, with momentum k_{trans} and centered at $x_0 = R_0 - r_0/2 = 8$ a_0, as shown in panel (b); see eq 42. The distance R_0 (= 7.29 a_0) between the mean values of the center of mass of the Cl_2 and H_2 molecules and the Jakobi coordinates x, y (= H_2 bond lengths), and z (= center of mass of the collinear Cl−H−H system with corresponding Cartesian coordinates q_1(= $r/2$), q_2, q_3) are also illustrated in the insets.

the Cl_2 molecule relative to the *para*-H_2-crystal will also be considered. The Cl atom at q_1 attacks the neighboring reactant $H_2(v=1)$ within less than 100 fs; coherent effects of the other, entangled Cl atom which moves to the opposite direction are not considered in our model. On this time scale, the *para*-H_2-crystal is considered as frozen, that is, we describe photodissociation of Cl_2 by means of a one-dimensional (1d) model which accounts for the increasing bond distance r, similar to the gas phase. This model of the quasi-unperturbated photodissociation is used, however, just for sufficiently small values, $r < r_a$, where the interaction between the dissociated Cl atoms and the neighboring H_2 molecules are negligible. This approximation is extrapolated from analogous systematic investigations of elementary photoinduced processes of dihalogens in rare gas matrixes.[25−27] Accordingly, photodissociation induces an avalanche of processes with increasing degrees of freedom, starting from the quasi-1d stretch of the dissociative bond during the first ∼50−100 fs, similar to the free molecule, followed by dynamical effects of interactions with the nearest neighboring atoms, which invoke few additional degrees of freedom (d.o.f.) during the first few hundred femtoseconds, until the subsequent high-dimensional energy dissipation during much longer time scales.

(v) Fifth, for step 3 of the three-step model, we anticipate that the subsequent reaction 1 occurs within a few hundred femtoseconds. Again, on this time scale, the rest of the *para*-H_2 crystal is considered as frozen, that is, we focus on the reactive system of the atoms Cl−H−H embedded in the *para*-H_2 solid, with reduced dimensionality; see also item (viii).

(vi) Sixth, after photoexcitation of $Cl_2(C\ ^1\Pi_u)$ in solid *para*-H_2, the entire system is in an electronic excited state, that is, reaction 1 should be treated rigorously as a process in that excited electronic state. Instead, we consider reaction 1 as if it starts from the electronic ground state of the reactants Cl + $H_2(v=0) \triangleq Cl(^2P_{3/2}) + H_2(X^1\Sigma_g^+,v)$ in solid *para*-H_2. This simplification suggests treating steps 2 and 3 separately, albeit with a "link". For convenience, we shall often drop the electronic quantum numbers.

(vii) Seventh, the interaction of the reactive subsystem Cl−H−H in its electronic ground state is described using a London−Eyring−Polanyi−Sato (LEPS) potential energy surface (PES)[28−31] with parameters fitted to the ab initio PES of Capecchi and Werner,[17] neglecting effects of van der Waals minima in the reactant configuration (compare ref 16) or nonadiabatic couplings to other near-degenerate PESs. Detailed quantum dynamics simulations of the Cl + H_2 reaction in the gas phase by Mahapatra,[20] employing six coupled PESs in full dimensionality, have shown that this simplification reduces the overall reaction rates because any transitions to the other coupled PESs turn out to be essentially nonreactive. This supports our previous conjecture (see item (i)), that is,

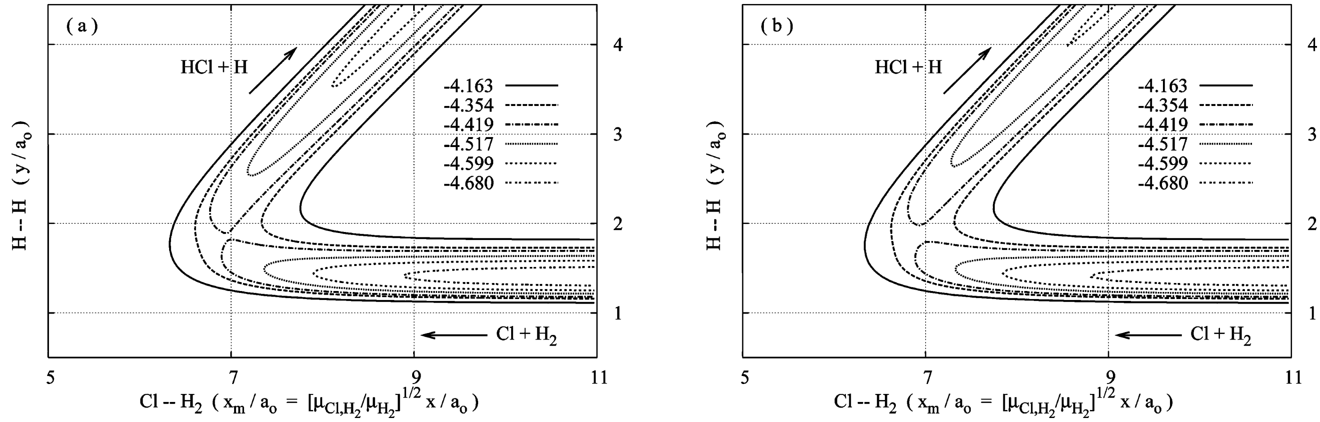

Figure 2. London−Eyring−Polanyi−Sato (LEPS[28−31]) potential energy surface (PES) for the model $Cl + H_2 \rightarrow HCl + H$ reaction. Equipotential contours are shown using mass-weighted coordinates (cf. eqs 6 and 50), where $\mu_{Cl,H_2}/\mu_{H_2} = 3.782$. (a) Barrier height and location fitted to the values of the ab initio PES of Capecchi and Werner.[17] (b) Empirical LEPS PES designed by Baer.[14]

the reaction probability $P_{v=1}$ for our model should be considered as an upper limit to the experimental one. Gratifyingly, the present LEPS PES is similar to the empirical LEPS PES, which had been derived by Baer[14] for simulations of experimental rate coefficients of the reaction in the gas phase;[15] compare Figure 2a and b. The recent investigations by Wang et al.[21] point to higher reaction probabilities for electronic excited chlorine atoms $Cl(^2P_{1/2})$ at low collision energies; these results are stimulating, as will be discussed in the Conclusions section, but they do not affect the present model simulations of the experiments of the group of D. T. Anderson, which prepare the chlorine atoms selectively in the ground state $Cl(^2P_{3/2})$.[1]

(viii) Eighth, the present LEPS PES favors a collinear reaction from the reactants via a potential barrier ($E^{\ddagger} \approx 0.330$ eV, also referred to as the transition state ‡) to the products, in accord with the ab initio PES of Capecchi and Werner[17,18] and the LEPS PES of Baer.[14] As a consequence, the reactive system is modeled by means of just three collinear coordinates q_1, q_2, and q_3 for atoms Cl, H, and H, respectively (cf. Figure 1b). An equivalent set of Jacobi coordinates is x for the distance from Cl to the center of mass of H_2, y for the H_2 bond lengths, and z for the center of mass of Cl−H−H relative to the *para*-H_2 crystal

$$\begin{pmatrix} x \\ y \\ z \end{pmatrix} = \begin{pmatrix} -1 & 0.5 & 0.5 \\ 0 & -1 & 1 \\ c_1 & c_2 & c_3 \end{pmatrix} \begin{pmatrix} q_1 \\ q_2 \\ q_3 \end{pmatrix} \quad \text{or}$$

$$\begin{pmatrix} q_1 \\ q_2 \\ q_3 \end{pmatrix} = \begin{pmatrix} -c_{23} & 0 & 1 \\ c_1 & -0.5 & 1 \\ c_1 & 0.5 & 1 \end{pmatrix} \begin{pmatrix} x \\ y \\ z \end{pmatrix} \quad (6)$$

where $c_1 = m_{Cl}/M$, $c_2 = c_3 = m_H/M$, $c_{23} = c_2 + c_3$, and $M = m_{Cl} + 2m_H$. Note that the reduction to just three d.o.f. is also supported by the fifth assumption.

(ix) Nineth, the corresponding initial wave function of the reactive system at time $t = t_0$ is assumed to separate into parts for the Cl atom and the H_2 molecule. The wave fuction for the Cl atom is characterized by the initial momentum $\hbar k$ and width Δq_1 (which depend on the UV laser frequency ω and on its duration τ, respectively, and also on the width ΔR_{Cl_2} of its distribution in an Einstein-type cell). The wave function for the H_2 molecule depends on the vibrational quantum number v of pre-excitation and on the widths ΔR_{H_2} of its distribution in the Einstein cell

TABLE 1: Parameters of the LEPS Potential Energy Surface[a] of the $Cl(^2P_{3/2}) + H_2 \rightarrow HCl + H$ Reaction

	H_2		HCl	
reactant/product molecule	this work[b]	ref 14	this work[b]	ref 14
D/eV[c]	4.748	4.747	4.629	4.616
y_e/a_0[d]	1.402	1.401	2.406	2.406
β/a_0^{-1}[e]	1.028	1.027	0.989	0.988
S[f]	0.170	0.167	0.183	0.187

[a] Compare ref 31. [b] Fitted to the ab initio potential of ref 17. Morse parameters for H_2 and HCl adapted from refs 34 and 35, respectively. [c] Morse potential well depths. [d] Morse potential equilibrium bond distance. [e] Morse potential parameter. [f] Sato parameters; compare refs 30 and 31.

$$\Psi_{Cl-H-H}(q_1, q_2, q_3, t_0) = \Psi_{Cl,k(\omega),\Delta q_1(\tau,\Delta R_{Cl_2})}(q_1, t_0) \cdot \Psi_{H_2,v,\Delta R_{H_2}}(q_2, q_3) \quad (7)$$

Obviously, the model cannot describe complementary dynamical effects, for example, the transformation from quasi-free rotation of the reactant *para*-$H_2(v,J=0)$ to libration or bending vibrations of the complex Cl−H−H close to the transition state.

Further discussions of these assumptions or approximations (i)−(ix) are in the following sections. Next, we derive and specify the corresponding three-step model.

B. Step 1: Vibrational Pre-excitation of $H_2(v=1)$ by IR Irradiation of the *para*-H_2 Crystal. Using the Einstein model, the initial wave function describing the reactant molecule $H_2(v)$ embedded in its Einstein cell is[22]

$$\Psi_{H_2,v,\Delta R_{H_2}}(q_2, q_3) = \Psi_v(y)\Psi_{\Delta R_{H_2}}(R) \quad (8)$$

where $\Psi_v(y)$ denotes the vibrational eigenfunction of $H_2(v)$, whereas $\Psi_{\Delta R_{H_2}}(R)$ describes the motion of the center of mass (R) of the H_2 molecule in the Einstein cell. Specificly, the vibration of H_2 is modeled as a Morse oscillator, with parameters D_{H_2}, β_{H_2}, and y_{e,H_2} listed in Table 1. The corresponding force constant is

$$\mu_{H_2}\omega_{H_2}^2 = 2D_{H_2}\beta_{H_2} \tag{9}$$

with reduced mass $\mu_{H_2} = m_H m_H/(m_H + m_H) = m_H/2$ and vibrational frequency ω_{H_2}. Accordingly, the $\Psi_v(y)$ are the Morse oscillator wave functions. The related vibrational levels are

$$E_{H_2,v} = -D_{H_2} + (v + 0.5)\hbar\omega_{H_2} - \frac{((v + 0.5)\hbar\omega_{H_2})^2}{4D_{H_2}} \tag{10}$$

We note in passing that the product molecule HCl(v') is also described as a Morse oscillator, with corresponding parameters as specified in Table 1 and expressions for the force constant and energy levels $E_{HCl,v'}$ analogous to eqs 9 and 10.

Furthermore

$$\Psi_{\Delta R_{H_2}}(R) \approx N_{H_2} \cdot e^{-0.5(R - R_0)^2/\Delta R_{H_2}{}^2} \tag{11}$$

is adapted from ref 22, that is, it is approximated as a Gaussian, centered at $R_0 = 7.29$ a$_0$ from the center of mass of the neighboring Cl$_2$ molecule, with width parameter $\Delta R_{H_2} = 1.21$ a$_0$. The corresponding density $\rho_{\Delta R_{H_2}}(r) = |\Psi_{\Delta R_{H_2}}(R)|^2$ has the fwhm = 2.01 a$_0$; compare item (ii).

C. Step 2: Generation of the Reactant Cl($^2P_{3/2}$) Atom by UV Photodissociation of Cl$_2$. The model of the second step, near-resonant UV photoexcitation and subsequent photodissociation

$$Cl_2(X^1\Sigma_g^+, v = 0) \rightarrow Cl_2(C^1\Pi_u) \rightarrow 2Cl(^2P_{3/2}) \tag{12}$$

starting from the Cl$_2$ molecule in the vibrational ground state $v = 0$ of the electronic ground state X = X $^1\Sigma_g^+$, employs the 1d potential energy curves $V_X(r)$ and $V_C(r)$ for the electronic states X and C = C $^1\Pi_u$ of Cl$_2$ in the gas phase, respectively, versus the bond distance in the molecular frame, $r = 2q_1$ (for effects of the motions of the c.o.m. of Cl$_2$ relative to the crystal, see subsection E). The $V_X(r)$ and $V_C(r)$ are shown in Figure 1, adapted from refs 32 and 33. We assume that this 1d model of the quasi-free Cl$_2$ molecule or two Cl atoms is valid until the chlorine atom at q_1 enters the domain of significant interaction with the neighboring H$_2$(v) molecule. According to the LEPS potential which has been fitted to the ab initio PES of ref 17, the spatial domain of validity is thus $0 < q_1 \lesssim R_0 - 4a_0 \approx 3a_0$ (cf. item (iii) and Figure 2) or $0 < r < 2 \cdot 3a_0 \approx 6a_0$; see also Figure 1. The corresponding temporal domain of validity of the 1d model is the time it takes the Cl−Cl bond distance r to enter this interaction domain, $r \gtrsim 6a_0$. This temporal domain is on the order of ~50−100 fs; the details depend not only on the dissociation dynamics of the photoexcited Cl$_2$ molecule but also on the parameters of the UV laser pulse which is used for photodissociation, in particular, on its frequency ω and duration τ.

The effects of the UV laser pulse are evaluated by means of quantum dynamics simulations of the photodissociation process. For this purpose, we solve the time-dependent 1d Schrödinger equation for the two nuclear wave functions which evolve on the adiabatic PES for the two lowest electronic singlet states; compare Figure 1 (i.e., neglecting, e.g., spin−orbit couplings to neighboring triplet states; for comparison, see ref 36)

$$i\hbar\frac{d}{dt}\begin{pmatrix}\Psi_X(r,t)\\ \Psi_C(r,t)\end{pmatrix} = \begin{pmatrix}H_{XX} & H_{XC}(t)\\ H_{CX}(t) & H_{CC}\end{pmatrix}\begin{pmatrix}\Psi_X(r,t)\\ \Psi_C(r,t)\end{pmatrix} \tag{13}$$

The wave functions $\Psi_X(r,t)$ and $\Psi_C(r,t)$ are propagated using the split operator and fast Fourier transform (FFT) methods of ref 37 in the domain $r \gtrsim 3$ a$_0$, with spatial and temporal grid parameters $\Delta r = 0.02$ a$_0$ and $\Delta t = 0.5\ \hbar/E_h = 0.012$ fs. Specifically, the diagonal elements H_{kk}(k = X or C) of the Hamiltonian are given by the sums of the kinetic energy operator plus the diabatic potential energy curves adapted from refs 32 and 33

$$H_{kk} = p_r^2/(2\mu_{Cl_2}) + V_k(r) \tag{14}$$

with reduced mass of the two dissociated chlorine atoms, $\mu_{Cl_2} = m_{Cl}/2$. The off-diagonal elements are

$$H_{XC}(t) = H_{CX}(t) = -d_{CX}(r) \cdot E(t) \tag{15}$$

where $d_{CX}(r)$ denotes the transition dipole for UV transitions between states X$^1\Sigma_g^+$ and C$^1\Pi_u$, adapted from ref 33 and

$$E(t) = E_0 \cdot s(t)\cos(\omega t + \eta) \tag{16}$$

is the component of the electric field causing UV photoexcitation perpendicular to the molecular axis, with field amplitude E_0, shape function $s(t)$, UV frequency ω, and phase η. For the present application, we employ the ubiqitious Gaussian shape function

$$s(t) = e^{-[(t - 2\tau)/\Delta t]^2} \tag{17}$$

which has its maximum (= 1) at time $t = 2\tau$, with corresponding maximum intensity, $I_{max} = \varepsilon_0 c E_0^2$. The full widths at half-maximum τ of the intensity profile $I(t) = \varepsilon_0 c E_0^2 s(t)^2$ defines the laser duration $\tau = (2\ln 2)^{1/2}\Delta t = 1.177\Delta t$. It is related to the spectral widths Γ according to $\Gamma\tau = 4 \cdot \ln 2\hbar = 2.773\hbar$. In the subsequent applications, we employ the laser parameters corresponding to the experimental UV photon energy $E_\omega = \hbar\omega = 3.782$ eV, which is near resonant to the X → C Franck−Condon transition.[1] This corresponds to the period $2\pi/\omega = 1.093$ fs of a single cycle, much shorter than the minimum value of the duration of the laser pulses which is employed in the subsequent applications, $\tau = 5$ fs. As a consequence, the phase η does not matter and is set to $\eta = 0$ for convenience. The electric field amplitude E_0 turns out to be irrelevant for the subsequent applications, as long as the related maximum intensity I_{max} is in the linear regime corresponding to dominant single-photon excitation. In the applications below, we employ $I_{max} \leq 7 \times 10^{12}$ W cm^{-2}. Finally, the durations of the laser pulses are varied systematically, from $\tau = 5$ fs to larger values, in order to extrapolate the results of continuous-wave (c.w.) excitation ($\tau \rightarrow \infty$). The corresponding spectral width decreases from its maximum value $\Gamma_{max} = 0.132$ eV to 0.

The propagation of the wave functions starts from the initial ($t = 0$) vibrational and electronic ground state

$$\begin{pmatrix}\Psi_X(r,t=0)\\ \Psi_C(r,t=0)\end{pmatrix} = \begin{pmatrix}\chi_{X,v=0}(r)\\ 0\end{pmatrix} \tag{18}$$

The correponding initial wave function $\chi_{X,v=0}(r)$ and its energy $E_{Cl_2,v=0} = E_{X,v=0}$ are shown in Figure 1, at the bottom of the potential energy curve $V_X(r)$. They are evaluated as a solution of the time-independent Schrödinger equation

$$H_{XX}\chi_{X,v=0}(r) = E_{X,v=0}\chi_{X,v=0}(r) \qquad (19)$$

using the Fourier Grid Hamiltonian Method (FGHM) of ref 37 and the same spatial grid as that for the time-dependent Schrödinger eq 13. The resulting nuclear wave functions $\Psi_{X,\omega,\tau}(r,t)$ and $\Psi_{C,\omega,\tau}(r,t)$ in the electronic ground and excited states depend on the frequency ω and the duration τ of the laser pulse. A snapshot of $\Psi_{C,\omega,\tau}(r,t_a)$ in the electronic excited C state, where $\tau = 20$ fs and t_a is 67 fs, that is, 37 fs after the peak of the UV laser pulse, is also shown in Figure 1. At the time t_a, it is centered at $r = r_a \approx 6\ a_0$, at the transition to the asymptotic (a) domain of the potential $V_C(r)$, and it is superimposed on a long horizontal line which indicates the asymptotic mean energy

$$E_C \approx E_{Cl_2,v=0} + \hbar\omega = 3.526\ \text{eV} \qquad (20)$$

in the electronic excited C state for the case of a short UV ($\lambda = 355$ nm) laser pulse, $\hbar\omega = 3.493$ eV. From here on, it moves toward larger values of $r \gtrsim 6\ a_0$, starting from the value for the mean total kinetic energy

$$\langle T\rangle \approx \Delta E = E_C - V_C(r \rightarrow \infty) = 1.058\ \text{eV} \qquad (21)$$

which is approximated by the photodissociation energy ΔE, that is, the difference of the mean energy E_C and the asymptotic energy equal to the potential $V_C(r\rightarrow\infty)$; compare Figure 1 and eq 20. Accordingly, the mean value of the momentum of the two chlorine atoms before reaction is determined by the laser frequency ω

$$\hbar k(\omega) = \sqrt{2\mu_{Cl_2}\langle T\rangle} \approx \sqrt{2\mu_{Cl_2}\cdot(E_{Cl_2,v=0} + \hbar\omega - V_C(r \rightarrow \infty))} \qquad (22)$$

In order to investigate the effects of the durations τ of the laser pulse on the wave functions, the two snapshots of $\Psi_{C,\omega,\tau}(r,t_a)$ centered at $r_a = 6\ a_0$ are compared in the inset of Figure 1 for $\tau = 10$ and 20 fs. Obviously, the wavepackets $\Psi_{C,\omega,\tau}(r,t)$ broaden as the durations τ of the UV laser pulses increase. This is a consequence of the fact that the laser pulse pumps partial waves of the initial $\chi_{X,v=0}(r)$ to the excited C states perpetually, as long as it is on. Those partial waves which are pumped first run ahead toward photodissociation, forming the "front" of $\Psi_{C,\omega,\tau}(r,t)$, whereas those parts which are pumped last are delayed, forming its "tail". The larger τ, the longer the corresponding distance between the front and the tail and, therefore, the broader the wave function $\Psi_{C,\omega,\tau}(r,t)$.

The inset 1a of Figure 1 also shows a comparison between the wave functions $\Psi_{C,\omega,\tau}(r,t_a)$ for $\tau = 10$ and 20 fs and corresponding Gaussian wavepackets $|\Psi_{G,\omega,\tau}(r,t_a)|^2$, labeled G. The agreement is seen to be nearly perfect, except for marginal deviations in the fronts and tails, which may be positive or negative depending on τ. Systematic investigations yield similar nearly Gaussian wavepackets $\Psi_{G,\omega,\tau}(r,t)$, for small values of τ. These are employed in the subsequent simulations of the quantum reaction dynamics. For longer durations τ, the Gaussian shapes appear after longer times. We conclude that the wave functions $\Psi_{C,\omega,\tau}(r,t_a)$ are well approximated by Gaussians close to $r = r_a = 6\ a_0$

$$\Psi_{G,k(\omega),\Delta r(\tau,t_a)}(r, t = t_a) = N_r(t_a)\cdot \exp\left[-\frac{1}{2}\left(\frac{r - r_a}{\Delta r(\tau, t_a)}\right)^2 + ik(\omega)(r - r_a) + i\delta(t_a)\right] \qquad (23)$$

where t_a is the time when the Gaussian (eq 23) is centered at $r = r_a \approx 6\ a_0$, $N_r(t_a)$ is the normalization at time t_a, $\Delta r(\tau,t_a)$ is its width at t_a depending on the laser pulse duration τ, $k(\omega)$ is the component of the wavevector along r (eq 22), and $\delta(t_a)$ is an irrelevant phase that we set to 0 for convenience. An important advantage of the Gaussian approximation is its analytical properties (see, e.g., ref 38); these will be exploited below.

D. The Link between Steps 2 and 3. Next, we construct a link between steps 2 and 3. For this purpose, we note that the domain of the potential energy curve $V_C(r)$ close to $r = r_a \approx 6\ a_0$ offers an "asymptotic transition domain", which has two important properties. On one hand, $V_C(r) \approx V_C(\infty)$ for $r \gtrsim 6\ a_0$, that is, it specifies the entrance into the asymptotic domain concerning photodissociation; see Figure 1. On the other hand, $r \lesssim 6\ a_0$ is the domain without any significant interactions of Cl and $H_2(v)$, or in other words, the "asymptotic transition domain" close to $r = 6\ a_0$ also specifies the exit from the asymptotic domain into the interaction domain, concerning the reaction $Cl + H_2(v) \rightarrow HCl + H$. As a consequence, when a UV laser pulse with frequency ω and duration τ produces the Gaussian-type wave functions $\Psi_{G,\omega,\tau}(r,t)$ (eq 23) in the "asymptotic transition domain" close to $r \approx 6\ a_0$ in step 2, then it may serve as a link between steps 2 and 3; on one hand, it has been generated in step 2, and on the other hand, it allows construction of the wave function which enters the interaction region of the $Cl + H_2$ reaction at the beginning of step 3 (for details, see subsection F). For short laser pulses ($\tau \lesssim 20$ fs), we can use $\Psi_{G,\omega,\tau}(r,t_a)$ centered at $r = r_a = 6\ a_0$ directly. For longer pulse durations $\tau \gtrsim 20$ fs, the widths of $\Psi_{G,\omega,\tau}(r,t)$ may exceed the rather narrow "asymptotic transition domain" close to $r \approx 6\ a_0$. To overcome this problem, at least in an approximate manner, we shall employ a trick which exploits the fact that for step 3, the history of $\Psi_{G,\omega,\tau}(r,t)$ before entering the "asymptotic interaction domain" does not matter. This allows us to construct a convenient artificial scenario which produces the same $\Psi_{G,\omega,\tau}(r,t)$ in the "asymptotic transition domain" as that for UV photodissociation, even for applications with larger widths of the $\Psi_{G,\omega,\tau}(r,t)$. Specifically, at the beginning of step 3, we shall employ a constant potential energy $V_G(r)$ in the domain $r \lesssim 6\ a_0$, which coincides with $V_C(r)$ in the "asymptotic interaction domain"; thus

$$V_G(r) = V_C(\infty) = \text{const} \quad \text{for } r \lesssim r_a = 6\ a_0 \qquad (24)$$

Next, we use the time-dependent Schrödinger eq 13 without a laser pulse but with the potential $V_C(r)$ replaced by the constant potential $V_G(r)$ (eq 24) in order to propagate $\Psi_{G,\omega,\tau}(r,t)$ from the "asymptotic interaction domain" back in time to $\Psi_{G,\omega,\tau}(r,t_0)$, which is centered at a smaller value r_0 of r at an earlier initial time t_0. A typical example is shown in Figure 1; see the Gaussian wavepacket which is denoted by $\Psi_G(t_0)$ and which is located at approximately $r_0 = 2R_0 - 8.00\ a_0 = -1.42\ a_0$. The analytical expression of this Gaussian wavepacket may be written using various equivalent forms; for convenience, we employ the form which is similar to eq 23; compare ref 38

$$\Psi_{G,k(\omega),\Delta r(\tau)}(r, t = t_0) = N_r \cdot \exp\left(-\frac{1}{2}\frac{(r - r_0)^2}{\Delta r(\tau)^2} + ik(\omega)\cdot(r - r_0) + i\delta\right) \quad (25)$$

where the parameters for the initial normalzation N_r, widths $\Delta r(\tau)$, momentum $k(\omega)$, and phase δ are determined such that upon forward propagation, the Gaussian (eq 25) at r_0 evolves on the constant potential (eq 24) to the same $\Psi_{G,\tau}(r,t)$ at r_a in the "asymptotic interaction domain" as that for the case of UV photodissociation, with frequency ω and duration τ; see Figure 1. Conservation of momentum for motion on a constant PES, eq 24, implies that $\hbar k(\omega)$ is the same as that specified in eq 22. The width parameters $\Delta r(\tau)$ at $t = t_0$ and $\Delta r(\tau, t = t_a)$ are related to each other by

$$\Delta r(\tau, t = t_a) = \Delta r(\tau)\cdot\sqrt{1 + \left(\frac{2\hbar(t_a - t_0)}{\Delta r(\tau)\cdot\mu_{Cl_2}}\right)^2} \quad (26)$$

where $t_a - t_0 = 100$ fs in the applications below. The normalizations and the phases are irrelevant for these applications; hence, we will not document the relations between N_r and δ (eq 25) and $N_r(t_a - t_0)$ and $\delta(t_a - t_0)$ (eq 23) here; compare ref 38. Again, the phase δ of this wavepacket is irrelevant for the subsequent applications and will be set to 0 for convenience.

The Gaussian wavepacket (eq 25) can be re-expressed in terms of the coordinates q_1 and q_{-1} of the two photodissociated chlorine atoms simply by replacing r with $r = q_1 - q_{-1}$ and with an equivalent expression for the center $r_0 = q_{1,0} - q_{-1,0}$ at time $t = t_0$. The result

$$\Psi_{G,k(\omega),\Delta r(\tau)}(q_1, q_{-1}, t = t_0) = N_r \cdot \exp\left(-\frac{1}{2}\frac{(q_1 - q_{-1} - (q_{1,0} - q_{-1,0}))^2}{\Delta r(\tau)^2}\right)\cdot \exp(ik(\omega)\cdot(q_1 - q_{1,0}) + i(-k(\omega))\cdot(q_{-1} - q_{-1,0})) \quad (27)$$

confirms that the two Cl atoms at q_1 and at q_{-1} ($= -q_1$) move with opposite momenta, and the values of the corresponding wave vectors are $k_1 = k$ and $k_{-1} = -k$, respectively, where $k = k(\omega)$ is specified in eq 22. Moreover, eq 27 shows that the two dissociative Cl atoms at q_1 and q_{-1} ($= -q_1$) are entangled, that is, the wave function (eq 27) cannot be written as a product of wave functions for the individual chlorine atoms. For our simple model which considers the reaction of just one of the chlorine atoms with the neighboring *para*-$H_2(v=1)$ molecule, we disregard this entanglement and write the corresponding approximate initial wave function for the Cl atom at q_1 with momentum $k_1 = \hbar k$ as

$$\Psi_{Cl,k(\omega),\Delta q_1(\tau)}(q_1, t = t_0) = N_{Cl}\cdot\exp\left(-\frac{1}{2}\frac{(q_1 - q_{1,0})^2}{\Delta q_1(\tau)^2} + ik(\omega)(q_1 - q_{1,0})\right) \quad (28)$$

with $q_{1,0} = r_0/2$ and normalization N_{Cl}. The corresponding expression for the momentum $p_1 = \hbar k_1(\omega) = p = \hbar k(\omega)$ yields the kinetic energy of the Cl atom at q_1

$$\langle T_1\rangle = \frac{p_1^2}{2m_{Cl}} = \frac{1}{2}\frac{p^2}{2\mu_{Cl_2}} = \frac{1}{2}\langle T\rangle \approx \frac{1}{2}\Delta E \quad (29)$$

As anticipated, the Cl atom which approaches the $H_2(v)$ molecule carries half of the photodissociation energy ΔE; needless to add, the other Cl atom carries the other half of ΔE. The different masses $\mu_{Cl_2} = m_{Cl}/2$ and m_{Cl} then imply that the velocity of the Cl_2 stretch along r is twice as fast as the motion of the single dissociated Cl along q_1. Likewise

$$\Delta r(\tau) = 2\Delta q_1(\tau) \quad (30)$$

The relation (eq 30) between the widths is derived from the requirement that the density

$$\rho_{Cl,k(\omega),\Delta q_1(\tau)}(q_1, t_0) = |\Psi_{Cl,k(\omega),\Delta q_1(\tau)}(q_1, t = t_0)|^2 \quad (31)$$

of the Cl atom at q_1 should agree with the corresponding density of the bond distance $r = q_1 - q_{-1}$, integrated over the coordinate of the other Cl atom at q_{-1}, subject to the constraint $q_1 = -q_{-1}$

$$\rho_{Cl,k(\omega),\Delta q_1(\tau)}(q_1, t) = \int dq_{-1}|\Psi_{G,k(\omega),\Delta r(\tau)}(q_1 - q_{-1}, t)|^2\cdot 2\delta\left(\frac{1}{2}(q_1 + q_{-1})\right) = N_r^2\cdot\exp\left[-\left(\frac{2(q_1 - q_{1,0})}{\Delta r(\tau)}\right)^2\right] \quad (32)$$

The widths $\Delta q_1(\tau, t_a)$ and the related $\Delta q_1(\tau)$ (for $\tau > 10$ fs) are listed in Table 2 for various values of τ of the durations of the laser pulses.

One readily sees that the widths $\Delta q_1(\tau, t_a)$ and $\Delta q_1(\tau)$ at t_0 are similar due to rather small dispersion during propagation from t_0 to t_a. In the following, we shall employ the slightly larger values of $\Delta q_1(\tau, t_a)$ instead of $\Delta q_1(\tau)$.

E. Effects of the *para*-H_2 Crystal on the Photodissociation of Cl_2. The photodissociation of a diatomic molecule in a matrix, such as Cl_2 embedded in a *para*-H_2 crystal, is quite different from that for the ideal gas. The latter has served as a reference in the derivations of subsections C and D for values of the bond distance $r \lesssim r_a \approx 6\ a_0$, where the interactions of the Cl atoms with the surrounding *para*-H_2 molecules are negligible. For larger values of r, one may, in principle, expect various consequences of significant interactions, such as the nuclear and electronic cage effects; for a review and recent extensions, see refs 39 and 36 respectively. In subsection F, we shall investigate the new phenomenon in the domain $r > r_a$, that is, the reaction of the photodissociated solute atom with the vibrationally pre-excited quantum solvent. Here, we focus on another effect which arises even for very small bond lengths, that is, the motion of the center of mass of the diatomic molecule relative to the crystal influences the widths of the wavepacket describing the photodissociated atom; alternative effects of the motions of the center of mass have been discovered in ref 40. For this purpose, we go beyond the previous scenario, which is adequate for the gas phase, that is, the center of mass of the Cl_2 molecule is at the origin, $0.5(r_1 + r_{-1}) = 0$. Instead, we shall assume that its mean value is at the origin, $\langle 0.5(r_1 + r_{-1})\rangle = 0$. Hence, there may be deviations from this mean value, described by the density $\rho_{Cl_2}(0.5(r_1 + r_{-1}))$. For simplicity, we shall assume that it is similar to the (normalized, N_{Cl_2}) distribution function of the center of mass of a

TABLE 2: Duration of the UV Laser Pulse τ and the Related Widths of the Wavepackets

τ/fs	$\Delta q_1(\tau,t_a)/a_0$[a]	$\Delta q_1(\tau)/a_0$[b]	$\Delta q_1(\tau,\Delta R_{Cl_2})/a_0$[c]	$\Delta x(\tau,\Delta R_{Cl_2},\Delta R_{H_2})/a_0$[d]
5	0.21	*e*	0.29	1.24
10	0.23	*e*	0.31	1.25
12	0.27	0.23	0.34	1.25
15	0.33	0.31	0.39	1.26
20	0.46	0.44	0.50	1.26
50	1.08	1.06	1.10	1.27
∞	∞	∞	∞	1.28

[a] Width of the Gaussian wavepacket $\Psi_{Cl,\omega,\tau}(q_1,t = t_a)$ when it is centered at $q_1 = q_{1a} = r_a/2 = 3$ a_0; compare eqs 23 and 30. [b] Width of the Gaussian wavepacket $\Psi_{Cl,\omega,\tau}(q_1,t = t_0)$ when it is back-propagated to $q_0 = -r_0/2 = -0.71$ a_0; compare 26, 28, and 30. [c] Width of the Gaussian wavepacket $\Psi_{Cl,\omega,\tau,\Delta R_{Cl_2}}(q_1,t_0)$, eqs 35 and 36. [d] Width of the translational wave function $\Psi_{Cl+H_2,k_{trans}(\omega),\Delta x(\tau,\Delta R_{Cl_2},\Delta R_{H_2})}$; compare eqs 41 and 43. [e] No back-propagation.

para-H_2 molecule in its Einstein cell, which is adapted from ref 22, except for the scaling (eq 5)

$$\rho_{Cl_2}(0.5(r_1 + r_{-1})) \approx N_{Cl_2} \cdot \exp\left[-\left(\frac{0.5(r_1 + r_{-1})}{\Delta R_{Cl_2}}\right)^2\right] \tag{33}$$

Accordingly, in eq 32, the delta function $\delta(0.5(q_1 + q_{-1}))$ which fixes the center of mass of the Cl_2 molecule to the origin is replaced by the distribution (eq 33). As a consequence, the density of the Cl atoms at q_1 becomes

$$\rho_{Cl,k(\omega),\Delta q_{Cl}(\tau,\Delta R_{Cl_2})}(q_1, t) = \int dq_1 |\Psi_{Cl,k(\omega),\Delta r(\tau)}(q_1 - q_{-1}, t)|^2 \cdot N_{Cl_2} \cdot \exp\left[-\left(\frac{0.5(q_1 + q_{-1})}{\Delta R_{Cl_2}}\right)^2\right] = N_{Cl} \cdot \exp\left[-\left(\frac{q_1 - q_{1,0}}{\Delta q_{Cl}(\tau, \Delta R_{Cl_2})}\right)^2\right] \tag{34}$$

with the relation for the widths

$$\Delta q_1(\tau, \Delta R_{Cl_2})^2 = \Delta R_{Cl_2}^2 + \Delta q_1(\tau)^2 \tag{35}$$

Hence, the initial wave function (eq 28) is modified as

$$\Psi_{Cl,k(\omega),\Delta q_1(\tau,\Delta R_{Cl_2})}(q_1, t_0) = N'_{Cl} \cdot \exp\left(-\frac{1}{2}\left(\frac{(q_1 - q_{1,0})}{\Delta q_1(\tau, \Delta R_{Cl_2})}\right)^2 + ik(\omega) \cdot (q_1 - q_{1,0})\right) \tag{36}$$

It is formally identical to eq 28, except that $\Delta q_1(\tau)$ is replaced by $\Delta q_1(\tau,\Delta R_{Cl_2})$. The corresponding modifications of the previous width parameters Δq_1 due to pure photodissociation by the widths ΔR_{Cl_2} for the motion of the center of mass of the Cl_2 molecule in an Einstein-type cell are documented in Table 2.

F. Step 3: The $Cl + H_2$ Reaction in a *para*-H_2 Crystal Induced by IR + UV versus Only UV Irradiation: The Initial Wave Function. Using the results, eqs 7−11 and 36 of the previous sections, we are now ready to set up the initial wave function for the reactive and nonreactive processes (eqs 1−3)

$$\Psi_{Cl-H-H}(q_1, q_2, q_3, t_0) = \Psi_{Cl,k(\omega),\Delta q_1(\tau,\Delta R_{Cl_2})}(q_1, t_0) \cdot \psi_{H_2,v,\Delta R_{H_2}}(q_2, q_3) = N'_{Cl} \cdot \exp\left[-\frac{1}{2}\left(\frac{(q_1 - q_{1,0})}{\Delta q_1(\tau, \Delta R_{Cl_2})}\right)^2 + ik(\omega)(q_1 - q_{1,0})\right] \cdot \Psi_v(q_3 - q_2) \cdot N_{H_2} \cdot \exp\left[-\frac{1}{2}\left(\frac{0.5(q_2 + q_3) - R_0}{\Delta R_{H_2}}\right)^2\right] \tag{37}$$

It consists of the product of the wave functions for the photodissociated Cl atom times the vibrational (Morse) eigenfunction of the H_2 molecule in the vibrational state v, depending on the H_2 bond length $y = q_3 - q_2$, times the wave functions which describes the motion of the center of mass of H_2 at $R = 0.5(q_2 + q_3)$ in its Einstein cell relative to the *para*-H_2 crystal. The effects of the UV laser pulse (frequency ω and duration τ) on the wave function for Cl (i.e., on its momentum and widths, respectively) are indicated by the notation. In the case of the "only UV" experiment, the quantum number for the vibrational wave function is $v = 0$. Otherwise, for the IR + UV experiment, the IR laser achieves vibrational pre-excitation, $v = 1$.

Next, we switch from Cartesian coordinates q_1, q_2, q_3 of the atoms Cl, H, H to Jacobi coordinates x, y, z; compare eq 6 and Figure 1. The reduced and total masses associated with the translational and vibrational motions along x and y and the motion of the c.o.m. are $\mu_{Cl,H_2} = m_{Cl} \cdot 2 \cdot m_H/M$, $\mu_{H_2} = m_H/2$, and M, respectively. The wave function (eq 37) is thus rewritten as

$$\tilde{\Psi}_{Cl-H-H}(x, y, z, t_0) = N'_{Cl} \cdot \exp\left[-\frac{1}{2}\left(\frac{-c_{23}(x - x_0) + (z - z_0)}{\Delta q_1(\tau, \Delta R_{Cl_2})}\right)^2 + ik(\omega) \cdot (-c_{23}(x - x_0) + (z - z_0))\right] \cdot \Psi_v(y) \cdot N_{H_2} \cdot \exp\left[-\frac{1}{2}\left(\frac{c_1(x - x_0) + (z - z_0)}{\Delta R_{H_2}}\right)^2\right] \tag{38}$$

where

$$\begin{pmatrix} x_0 \\ y_0 \\ z_0 \end{pmatrix} = \begin{pmatrix} -1 & 0.5 & 0.5 \\ 0 & -1 & 1 \\ c_1 & c_2 & c_3 \end{pmatrix} \begin{pmatrix} q_{1,0} \\ q_{2,0} \\ q_{3,0} \end{pmatrix} \tag{39}$$

in analogy with eq 6; $q_{1,0} = -0.71$ a_0 is the center of the Gaussian wavepacket representing the photodissociated Cl atom in the *para*-H_2 crystal at time t_0, as determined in subsection E, and $q_{2,0} = q_{3,0} = R_0 = 7.29$ a_0. The corresponding values of x_0, y_0, and z_0 are 8.00, 0.00, and −0.28 a_0, respectively. We assume that initially, the reactive or nonreactive processes of the Cl−H−H system are governed by the motions along coordinates x and y, whereas the motion along z will affect the dynamics at later times, for example, during dissipation of the c.o.m. energy into the *para*-H_2 crystal. For simplicity, we neglect, therefore, any effects of the motion along z. Formally, this approximation is made by setting $z = z_0$ in eq 38. Note that rigorously, the motion of the c.o.m. of the Cl−H−H system versus the *para*-H_2 crystal is entangled with the motion along x (eq 38), that is, it cannot be separated; this is different from the ubiquitious separation of the c.o.m. in the gas phase. As a consequence, the initial wave function (eq 38) for the total model system is reduced to a product of translational times vibrational wave functions

$$\Psi_{\mathrm{Cl+H_2}}(x,y,t_0) = \Psi_{\mathrm{Cl+H_2}(v),k(\omega),\Delta x(\tau,\Delta R_{\mathrm{Cl_2}},\Delta R_{\mathrm{H_2}})}(x,y,t_0) = N_{\mathrm{Cl}}(t_0)\cdot\exp\left[-\frac{1}{2}\left(\frac{c_{23}(x-x_0)}{\Delta q_1(\tau,\Delta R_{\mathrm{Cl_2}})}\right)^2 - \mathrm{i}k(\omega)\cdot c_{23}(x-x_0)\right]\cdot\Psi_v(y)\cdot N_{\mathrm{H_2}}\cdot\exp\left[-\frac{1}{2}\left(\frac{c_1(x-x_0)}{\Delta R_{\mathrm{H_2}}}\right)^2\right] = \Psi_{\mathrm{trans},k_{\mathrm{trans}}(\omega),\Delta x(\tau,\Delta R_{\mathrm{Cl_2}},\Delta R_{\mathrm{H_2}})}(x,t_0)\cdot\Psi_v(y) \quad (40)$$

where

$$\Psi_{\mathrm{trans},k_{\mathrm{trans}}(\omega),\Delta x(\tau,\Delta R_{\mathrm{Cl_2}},\Delta R_{\mathrm{H_2}})}(x,t_0) = N_{\mathrm{Cl+H_2}}\cdot\exp\left[-\frac{1}{2}\left(\frac{x-x_0}{\Delta x(\tau,\Delta R_{\mathrm{Cl_2}},\Delta R_{\mathrm{H_2}})}\right)^2 + \mathrm{i}k_{\mathrm{trans}}(\omega)(x-x_0)\right] \quad (41)$$

For convenience, we employ the ubiquitious normalization $N_{\mathrm{Cl+H_2}} = (1/\pi\Delta x^2)^{1/4}$ such that the wave function $\Psi_{\mathrm{Cl+H_2}}$, eq 40, is renormalized, irrespective of the laser intensity. This allows straightforward calculations of the reaction probabilities for comparison with the experimental results; see eq 53. The translational wave function (eq 41) is illustrated in Figure 1a. It depends on the translational momentum

$$\hbar k_{\mathrm{trans}}(\omega) = -c_{23}\hbar k(\omega) \quad (42)$$

which is determined by the laser frequency ω, and on the translational widths Δx. The latter is determined by the laser duration τ and the widths $\Delta R_{\mathrm{Cl_2}}$ and $\Delta R_{\mathrm{H_2}}$ of the distributions of the c.o.m.'s of the Cl_2 and H_2 molecules in their Einstein-(type) cells

$$\begin{aligned}\frac{1}{\Delta x^2} &= \frac{c_{23}^2}{\Delta q_1(\tau,\Delta R_{\mathrm{Cl_2}})^2} + \frac{c_1^2}{\Delta R_{\mathrm{H_2}}^2}\\ &= \frac{c_{23}^2}{\Delta R_{\mathrm{Cl_2}}^2 + \Delta q_1(\tau)^2} + \frac{c_1^2}{\Delta R_{\mathrm{H_2}}^2}\end{aligned} \quad (43)$$

The modifications of q_1 by the effect of the width $\Delta R_{\mathrm{H_2}}$ yielding Δx are documented in Table 2. Apparently, Δx is dominated by $\Delta R_{\mathrm{H_2}}$, with rather small influence of the duration of the laser pulse. This is due to the large and small mass ratios $c_1 = m_{\mathrm{Cl}}/M$ and $c_{23} = 2m_{\mathrm{H}}/M$ in eq 43, respectively. Likewise, k_{trans} depends also on the masses of the atoms. Accordingly, the initial wave function (eq 40) consists of a Gaussian wavepacket traveling along x with translational momentum $-c_{23}\hbar k(\omega)$, which is reduced by a factor of $c_{23} = 2m_{\mathrm{H}}/M$, compared to the momentum which is generated in the dissociated Cl atom by the UV laser pulse. Also note the minus sign of the momentum, that is, the photodissociated stretch of the Cl_2 bond distance $r = 2r_1$ corresponds to a decrease of the distance x between the Cl atom and the c.o.m. of the H_2 molecule. The corresponding translational energy is

$$E_{\mathrm{trans}} = ((2m_{\mathrm{H}}/M)\hbar k(\omega))^2/2(2m_{\mathrm{H}}m_{\mathrm{Cl}})/M \quad (44)$$

The small mass ratio $m_{\mathrm{H}}/M = 0.0273$ implies that this is only a small fraction of the initial kinetic energy of the two dissociated Cl atoms

$$E_{\mathrm{trans}} = E_x = \frac{m_{\mathrm{H}}}{M}\cdot\Delta E(\omega) \quad (45)$$

compared with eq 21. For the experiment[1]

$$E_x = 0.0273\Delta E(\omega) = 0.0288\ \mathrm{eV} \quad (46)$$

G. Step 3: The Cl + H_2 Reaction in a *para*-H_2 Crystal Induced by IR + UV versus Only UV Irradiation: Quantum Dynamics. The wave functions $\Psi_{\mathrm{Cl+H_2}}(x,y,t)$ representing the reactive and nonreactive processes (eqs 1−3) in solid *para*-H_2 are propagated, in the frame of the present simple model, as solutions of the time-dependent Schrödinger equation

$$\mathrm{i}\hbar\frac{\mathrm{d}}{\mathrm{d}t}\Psi_{\mathrm{Cl+H_2}(v),k_{\mathrm{trans}}(\omega),\Delta x(\tau,\Delta R_{\mathrm{Cl_2}},\Delta R_{\mathrm{H_2}})}(x,y,t) = H\Psi_{\mathrm{Cl+H_2}(v),k_{\mathrm{trans}}(\omega),\Delta x(\tau,\Delta R_{\mathrm{Cl_2}},\Delta R_{\mathrm{H_2}})}(x,y,t) \quad (47)$$

starting from the initial wave function (eqs 40 and 41), which has been determined in the previous sections, depending on the laser frequency ω and duration τ and on the widths of the distributions $\Delta R_{\mathrm{Cl_2}}$ and $\Delta R_{\mathrm{H_2}}$ of the Cl_2 and H_2 molecules in their Einstein(-type) cells, as indicated by the notation. Since we have separated the initial steps 1, 2, and 3, the definition of the initial time t_0 (which is determined in step 2) is irrelevant for the subsequent collision and reaction dynamics and will be reset to $t_0 = 0$.

The Hamiltonian

$$H = T_{x,y} + V(x,y) \quad (48)$$

in eq 47 accounts for the kinetic energy operator

$$T_{x,y} = -\frac{\hbar^2}{2\mu_x}\frac{\mathrm{d}^2}{\mathrm{d}x^2} - \frac{\hbar^2}{2\mu_y}\frac{\mathrm{d}^2}{\mathrm{d}y^2} \quad (49)$$

for the (initially translational and vibrational) motions along x and y, respectively, and for the potential energy surface $V(x,y)$ depending on x and y. The associated reduced masses are $\mu_x = \mu_{\mathrm{Cl,H_2}}$ and $\mu_y = \mu_{\mathrm{H_2}}$. Equation 6 implies that $V(x,y)$ is an implicit function of all bond distances in the collinear configuration, as shown in Figure 1a.

For convenience, $V(x,y)$ is modeled here as a LEPS PES[28−31] fitted to the ab initio PES of Capecchi and Werner,[17] as shown in Figure 2a using mass-weighted coordinates x_{m}, y, where

$$x_{\mathrm{m}} = \sqrt{\mu_{\mathrm{Cl,H_2}}/\mu_{\mathrm{H_2}}}\cdot x \quad (50)$$

The advantage of the presentation of the PES $\tilde{V}(x_m,y)$ in terms of x_m, y is that the kinetic energy operator (eq 49) can be rewritten with a single mass[29,31]

$$\tilde{T}_{x_m,y} = -\frac{\hbar^2}{2\mu_y}\left(\frac{d^2}{dx^2} + \frac{d^2}{dy^2}\right) \tag{51}$$

ready for interpretations in terms of the wavepacket dynamics representing a ball with mass μ_y running in the potential; this will be exploited in section III when we relate the results to the Polanyi rules.[41,42] The LEPS PES depends on rather few LEPS parameters, which are listed in Table 1. They include the parameters for the Morse potentials of the asymptotic reactant and product molecules, H_2 and HCl, adapted from refs 34 and 35, plus the corresponding so-called Sato parameters.[31] Since the Morse parameters are necessary in order to account for the asymptotic domains of the reaction $Cl + H_2 \rightarrow Cl{-}H{-}H^{\ddagger} \rightarrow HCl + H$, there are only the two Sato parameters for sculpting the LEPS in the interaction domain close to the "transition state" ‡. We have used these Sato parameters in order to fit two important properties of the ab initio PES of Capecchi and Werner, that is, the barrier height $E^{\ddagger} = 0.330$ eV at ‡ and its position $y^{\ddagger}$ along the coordinate y. Gratifyingly, these two requirements also yield excellent agreement for the position $x^{\ddagger}$ of ‡ along the coordinate x.

Figure 2 compares the present LEPS PES $\tilde{V}(x_m,y)$, which has been fitted to the ab initio PES of Capecchi and Werner[17] (panel a), with the empirical LEPS PES that has been designed by Baer[14] in order to account for early experimental results of Persky and co-workers[13,15] (panel b). The parameters for Baer's LEPS PES are also listed in Table 1. The agreement is quite amazing and mutually rewarding; on one hand, it implies that the topology of the LEPS PES is reasonable, that is, using a LEPS PES for the present model investigation should be an adequate approximation (in view of all of the other model assumptions) to the significant parts of the ab inito PES that determine the reactivity of the $Cl + H_2$ reaction. This conjecture may even be extended to nonlinear configurations, that is, both the ab inito PES of refs 17 and 18 and the LEPS PES[31] support colinear approaches of the reactants. On the other hand, given the restricted form of the PES, its energetic properties and the dynamical consequences concerning the height of the barrier and its position are expected to be quantitative, within the frame of the present simple 2d model.

Some important energetic properties of the LEPS PES fitted to the ab initio PES of Capecchi and Werner[17] are illustrated in Figure 3, including the barrier height $E^{\ddagger}$ and the vibrational levels $E_{H_2,v}$ ($v = 0$, 1, and 2) and $E_{HCl,v'}$ ($v' = 0$, 1, 2, and 3) of the reactants and products, respectively. Obviously, the reaction is slightly endoergic, that is, the process (eq 2) starting from the vibrational ground state is nonreactive if the sum of the vibrational level $E_{H_2,v=0}$ plus the translational energy E_{trans} (see mark E_x in Figure 3) is below the threshold $E_{HCl,v'=0}$ (see mark E_a). One may anticipate, however, that even slightly higher translational energies ($E_{H_2,v=0} + E_{trans} = E_a$) will not be efficient because E_a is still below the barrier $E^{\ddagger}$ (see mark E_b). Hence, it will be necessary to supply additional energy in order to induce the reaction, either by means of vibrational energy of the reactant (see mark E_c for $E_{H_2,v=1} > E^{\ddagger}$), plus a small amount of translational energy (compare marks E_x and E_d for equal amounts of translational energy added to $E_{H_2}(v=0)$ or to $E_{H_2}(v=1)$, respectively), or as a rather large value of pure translational energy, such that $E_{H_2,\tilde{v}=0} + \tilde{E}_{trans} = E_d$; see again mark E_d and eq 4.

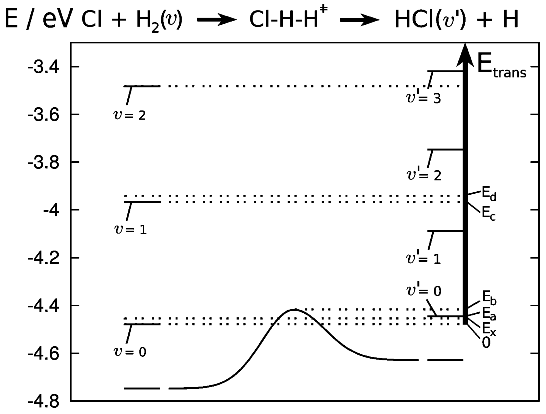

Figure 3. Energetics of the $Cl + H_2(v) \rightarrow Cl{-}H{-}H^{\ddagger} \rightarrow HCl(v') + H$ reaction. The profile of the PES versus the reaction path leads from the bottom of the reactant valley at $-D_{H_2}$ via the barrier ($E^{\ddagger} = 0.330$ eV above $-D_{H_2}$; cf. mark E_b) to the bottom of the product valley at $-D_{HCl}$ (schematic), according to the present LEPS PES fitted to the ab initio PES of Capecchi and Werner;[17] compare Figure 2a and Table 1. Also shown are the vibrational levels $E_{H_2,v}(v=0,1,2)$ and $E_{HCl,v'}(v' = 0,1,2,3)$ of the reactants and products, eq 10. The energy scale for the corresponding translational energies E_{trans} of the reactants $Cl + H_2(v=0)$ shows the related marks 0 ($\hat{=} E_{H_2,v=0}$), E_a ($\hat{=} E_{HCl,v'=0}$), and E_c ($\hat{=} E_{H_2,v=1}$). Also shown is the energy E_x which is available for translational motion of the reactants $Cl + H_2(v=0)$ due to photodissociation of the Cl_2 molecule in the electronic excited C state, embedded in the *para*-H_2 crystal, by a UV laser pulse with photon energy $E_\omega = 3.782$ eV (adapted from ref 1); compare Figure 1 and eqs 20, 21, and 45, as well as mark E_d for the energy $E_{H_2,v=1} + E_x$.

The 2d time-dependent Schrödinger equation (TDSE) (eq 47) is propagated using the coordinates x and y and the same techniques, adapted from ref 37, which have been employed previously for the 1d TDSE, eq 13. After the collision, the wave function is either scattered back toward the potential valley for the reactants or it penetrates into the potential valley for the products, $y > y_b \approx 3\ a_0$. The reaction probability $P_{v,\omega,\tau,\Delta R_{Cl_2},\Delta R_{H_2}}$ depending on the laser parameters and the parameters for the distributions of the Cl_2 and H_2 molecules in the crystal may be evaluated as time integrated fluxes j_{Cl+H_2} which enter the product domain, $y > y_b = 3\ a_0$, analogous to the method of ref 43. Here, we employ an alternative approach which is equivalent due to the continuity equation

$$\nabla j_{Cl+H_2} + \frac{\partial}{\partial t}\rho_{Cl+H_2} = 0 \tag{52}$$

that is, we determine the reaction probability by integrating the density of the wave function $\Psi_{Cl+H_2(v),k,\Delta x}(x,y,t\rightarrow\infty)$ in the asymptotic domain $y > y_b$ at sufficiently long times ($t \rightarrow \infty$) when the wave function has left the Cl−H−H interaction domain, either toward the products or toward the reactants

$$\begin{aligned} P_{Cl+H_2(v)\rightarrow HCl+H,k_{trans},\Delta x} &= \\ \int_0^{+\infty} dx \int_{y_b}^{+\infty} dy\ \rho_{Cl+H_2(v),k_{trans},\Delta x}(x, y, t \rightarrow \infty) &= \\ \int_0^{+\infty} dx \int_{y_b}^{+\infty} dy\ |\Psi_{Cl+H_2(v),k_{trans},\Delta x}(x, y, t \rightarrow \infty)|^2 & \end{aligned} \tag{53}$$

In practice, the integrals in eq 53 are restricted from infinite to finite domains which contain the significant contributions of the wave function $\Psi_{Cl+H_2(v),k,\Delta x}(x,y,t\rightarrow\infty)$. The method of eq 53 has two advantages, it avoids the calculation and integration of fluxes and it allows, in principle, a straightforward extension from calculations of total reaction probabilities to state-selective ones, $P_{\mathrm{Cl+H_2}(v)\rightarrow\mathrm{HCl}(v')+\mathrm{H},k,\Delta x}$. The latter are based on the fact that for reactants Cl + $H_2(v)$ with total energy $E_{\mathrm{tot}} = E_{\mathrm{H_2},v=0} + E_{\mathrm{trans}}$, the products HCl($v'$) + H with different vibrational quantum numbers v' have different partitionings of vibrational plus translational energies $E_{\mathrm{tot}} = E_{\mathrm{HCl}(v')} + E_{\mathrm{HCl+H,trans}'}$. As a consequence, the wavepacket $\Psi_{\mathrm{Cl+H_2}(v),k,\Delta x}$ branches into corresponding partial waves with different velocities, that is, rapid versus slow ones for products with low versus high vibrational quantum numbers, respectively. The integration (eq 53) can then be carried out separately for each of the partial waves, yielding the corresponding state specific $P_{\mathrm{Cl+H_2}(v)\rightarrow\mathrm{HCl}(v')+\mathrm{H},k,\Delta x}$. In the present paper, we do not use this option, but it is obvious from the subsequent results, which clearly demonstrate the separation of $\Psi_{\mathrm{Cl+H_2}(v),k,\Delta x}$ into various partial waves for products with different vibrational levels v'; analogous branchings are also observed for the nonreactive parts of the wave function; see Figures 4−7 below. These advantages of eq 53 are gained, however, at the expense of rather large domains for the wave function $\Psi_{\mathrm{Cl+H_2}(v),k,\Delta x}(x,y,t\rightarrow\infty)$ representing the products and reactants, calling for corresponding large grids for the numerical propagations. Note, however, that these large domains are just a numerical requirement for the method of eq 53, that is, they do not imply that the 2d wave function $\Psi_{\mathrm{Cl+H_2}(v),k,\Delta x}(x,y,t)$ enters the corresponding domains without any additional interactions with the *para*-H_2 crystal. The equivalent method of the corresponding integrated fluxes would, indeed, require propagation of $\Psi_{\mathrm{Cl+H_2}(v),k,\Delta x}(x,y,t)$ just in the interaction domain, without consideration of those asymptotic domains for the reactants or products.

III. Results and Discussions

The presentation of the results for the quantum dynamics simulations of the reactive and nonreactive processes (eqs 1−4) in solid *para*-H_2 starts with examples which are motivated by the experimental IR + UV versus "only UV" studies of eqs 1 and 2 by the group of D. T. Anderson.[1] For this purpose, we use exemplary snapshots of the time-dependent densities

$$\rho_{\mathrm{Cl+H_2}(v),k_{\mathrm{trans}},\Delta x}(x,y,t) = |\Psi_{\mathrm{Cl+H_2}(v),k_{\mathrm{trans}},\Delta x}(x,y,t)|^2 \quad (54)$$

for the wave functions $\Psi_{\mathrm{Cl+H_2}(v),k_{\mathrm{trans}},\Delta x}(x,y,t)$, which are calculated as solutions of the time-dependent Schrödinger eq 47, starting from corresponding initial wave functions $\Psi_{\mathrm{Cl+H_2}(v),k_{\mathrm{trans}},\Delta x}(x,y,t_0)$, eqs 40 and 41. They are illustrated by means of equidensity contours superimposed on equipotential contours for the LEPS PES; loosely speaking, we shall also refer to them as illustrations of the wave functions. These snapshots allow discovery of various effects of the reaction mechanism, which are related to the resulting reaction probabilities $P_{v,E_{\mathrm{trans}},\Delta x}$ depending on the initial vibrational quantum number v of the H_2 molecule, on the translational energy $E_{\mathrm{trans}} = (\hbar k_{\mathrm{trans}})^2/(2\mu_{\mathrm{Cl,H_2}})$ of the reactants Cl + $H_2(v)$ and on the corresponding translational width Δx. Subsequently, these examples will serve as references for the investigation of more general trends. Our quantum dynamics simulations will be used to analyze some important aspects of the experimental results.[1]

Consider first the wavepacket dynamics corresponding to the nonreactive process (eq 2), which is motivated by the "only UV" experiment of ref 1, as illustrated in Figure 4. Figure 4a shows the initial (time t_0 reset to $t_0 = 0$) density representing the reactants Cl + $H_2(v=0)$ with vibrational and translational energies $E_{\mathrm{H_2},v=0}$ and $E_{\mathrm{trans}}(\omega) = E_{\mathrm{x}}$ (eq 46) with UV photon energy $E_\omega = \hbar\cdot\omega = 3.493$ eV.[1] It is centered in the reactant valley of the PES at $x = 8$ a_0, $y = y_{\mathrm{H_2,e}}$, in accord with Figure 1a; see also Table 1. The translational width $\Delta x = 1.28$ a_0 of the initial wave function is close to the width $\Delta x(\tau,\Delta R_{\mathrm{Cl_2}},\Delta R_{\mathrm{H_2}})$, which is estimated for very long laser pulse durations in the frame of the present three-step model; compare eq 43 and the limit $\tau \rightarrow \infty$ in Table 2. The arrow in Figure 1a indicates the direction of the corresponding translational momentum

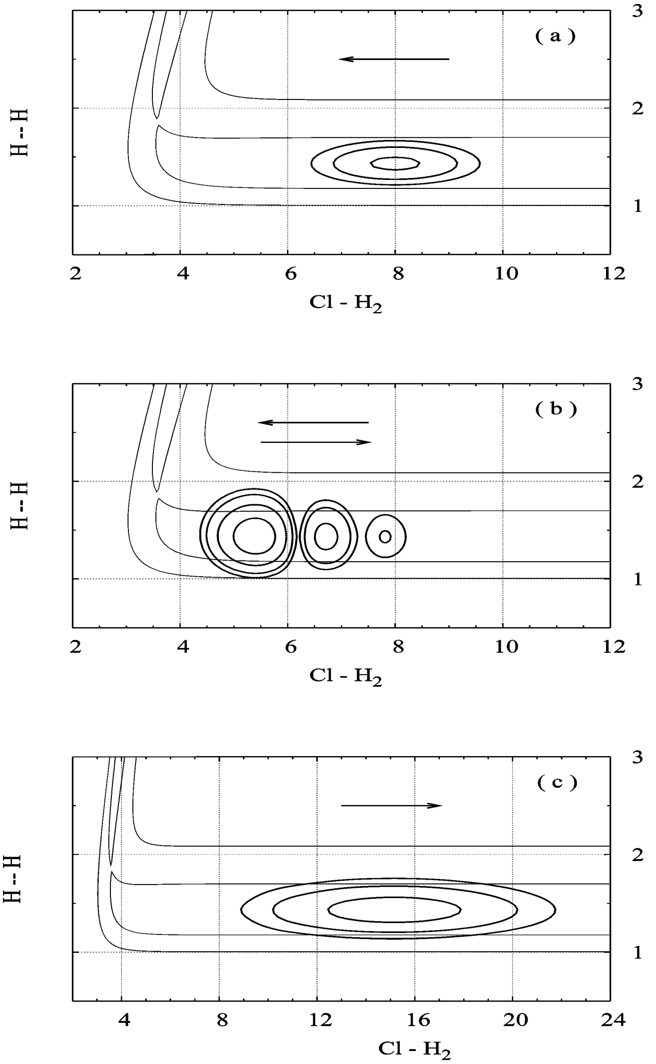

Figure 4. Quantum dynamics simulation of the elastic model collision Cl + $H_2(v=0) \rightarrow$ Cl + $H_2(v=0)$ (eq 2) with initial translational energy $E_{\mathrm{x}} = 0.030$ eV (eq 46), as provided by photodissociation of Cl_2 in the electronic excited C state by a UV laser pulse with photon energy $E_\omega = 3.493$ eV (adapted from ref 1; cf. Figures 1 and 3). The time evolution of the wavepacket $\Psi_{\mathrm{Cl+H_2}}(x,y,t)$ is illustrated by equidensity contours superimposed on equipotential contours for the LEPS potential energy surface (cf. Figure 2a) in terms of coordinate x for the Cl−H_2 distance between the Cl atom and the center of mass of the H_2 molecule and y for the H_2 bond length. Snapshot (a) shows the density of the initial wave function $\Psi_{\mathrm{Cl+H_2}}(x,y,t_0)$, centered at $x = 8$ a_0 and $y = y_{\mathrm{H_2,e}}$ (compare Figure 1a and eqs 40 and 41), assuming the momentum $k_{\mathrm{trans}}(\omega)$ generated by the laser pulse (eq 42) and the widths $\Delta x = 1.28$ a_0. The subsequent snapshots illustrate the wave function $\Psi_{\mathrm{Cl+H_2}}(x,y,t)$ during the rescattering from the potential barrier (b) ($t = 125$ fs) and on return to the (nonreactive) reactant configuration (c) ($t = 485$ fs). The relation of the simulated quantum dynamics and the "only UV" experiment of ref 1 is discussed in the text; the arrows indicate the directionality of the underlying processes. Note the different scales for the x coordinate. The wavepacket dynamics is determined in the interaction domain, $x \lesssim x_{\mathrm{a}} = R_0 - r_{\mathrm{a}}/2 = 4.29$ a_0, $y \lesssim y_{\mathrm{b}} = 3$ a_0. The complementary asymptotic domains serve for analysis; see the text.

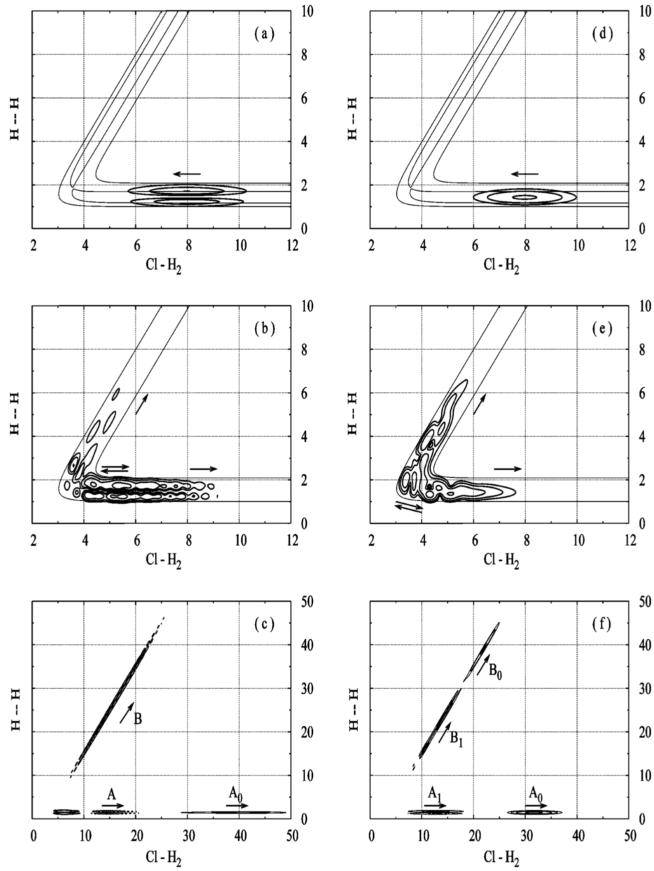

Figure 5. Left panels (a−c): Same as Figure 4 but for the $Cl + H_2(v{=}1) \rightarrow Cl + H_2$ reaction (cf. panel (c), with lobe labeled B of the wave function entering the potential valley of the products) competing against elastic collisions → $Cl + H_2(v{=}0)$ (lobe labeled A_0) and mainly inelastic collisions → $Cl + H_2(v{=}1)$ (lobe labeled A). The total energy is $E_{\mathrm{tot}} = E_{v=1} + E_{\mathrm{x}}$ (cf. eq 4 and Figure 3, mark E_{d}). The relation of the simulated quantum dynamics and the IR + UV experiment of ref 1 is discussed in the text. Right panels (d−f): Same as left panels (a−c) but starting from reactants $Cl + H_2(\tilde{v}{=}0)$ with the same total energy $E_{\mathrm{tot}} = E_{\tilde{v}=0} + \tilde{E}_{\mathrm{trans}}$. The snapshots (a), (b), (c), and (d), (e), (f) are taken at times of 0, 95, 395 and 0, 50, 240 fs, respectively.

$k_{\mathrm{trans}}(\omega)$ (eqs 22 and 42), that is, the initial wavepacket is moving toward the interaction region of the PES. Note that the mean energy of this wavepacket is below the reaction threshold, which, in turn, is below the reaction barrier (cf. marks $E_{\mathrm{x}} < E_{\mathrm{a}} < E_{\mathrm{b}}$ in Figure 3), that is, we expect that the initial wavepacket shown in Figure 4a cannot react to products HCl + H. This conjecture is confirmed by the subsequent snapshots of the wavepacket $\Psi_{Cl+H_2(v=0),k_{\mathrm{trans}}(\omega),\Delta x}(x,y,t)$ for $t = 125$ and 485 fs, shown in Figure 4b and c, respectively. Specifically, panel b shows the snapshot taken at the time when the tail of the wave function is still running toward the interaction region, whereas its front has already been reflected from the potential barrier such that it turns back to the reactant valley of the PES, without ever entering the domain of the products HCl + H at $y \approx y_{\mathrm{b}} = 3\ a_0$. The two opposite directions of the tail and front of the wavepacket are indicated by the two opposite arrows in Figure 4b. Their superposition gives rise to the interferences which are obvious from the nodal patterns of $\rho_{Cl+H_2(v=0),k_{\mathrm{trans}}(\omega),\Delta x}(x,y,t{=}125\ \mathrm{fs})$. The final effect, almost perfect elastic scattering, is illustrated in Figure 4c, that is, $\Psi_{Cl+H_2(v=0),k_{\mathrm{trans}}(\omega),\Delta x}(x,y,t)$ returns to the reactant domain of the PES, with reversed momentum and modest dispersion. The corresponding reaction probability is $P_{v=0,E_{\mathrm{trans}}(\omega),\Delta x} \approx 1.6 \times 10^{-5}$, within the numerical accuracy of the propagation. This is in semiquantitative agreement with the result $P_{v=0}$ ("only UV") ≈ 0.006 for the "only UV" experiment of ref 1; a possible reason for the small deviations of $P_{v=0,E_{\mathrm{trans}}(\omega)}$, Δx, or $P_{v=0}$ ("only UV") from 0 will be discussed below.

Next let us investigate the wavepacket dynamics corresponding to the reactive process (eq 1) which is motivated by the IR + UV experiment of ref 1, as illustrated in the left panels of Figure 5. For comparison with the nonreactive process (eq 2), the panels a−c are arranged analogous to Figure 4a−c. Specifically, Figure 5a shows the initial wave function $\Psi_{Cl+H_2(v=1),k_{\mathrm{trans}}(\omega),\Delta x}(x,y,t_0)$; it has the same parameters for the translational momentum $\hbar \cdot k_{\mathrm{trans}}(\omega)$ and for the width Δx as $\Psi_{Cl+H_2(v=0),k_{\mathrm{trans}}(\omega),\Delta x}(x,y,t_0)$ shown in Figure 4a, except that the initial vibrational quantum number is $v = 1$ (not $v = 0$), corresponding to the IR + UV (not "only UV") experiment of ref 1. The vibrational excitation is obvious from the nodal pattern of the density $\rho_{Cl+H_2(v=1),k_{\mathrm{trans}}(\omega),\Delta x}(x,y,t_0)$. As a consequence, the total (= vibrational plus translational) energy $E_{\mathrm{tot}} = E_{H_2,v=1} + E_{\mathrm{x}}$ of $\Psi_{Cl+H_2(v=1),k_{\mathrm{trans}}(\omega),\Delta x}(x,y,t_0)$ is much larger than $E_{H_2,v=0} + E_{\mathrm{x}}$ for $\Psi_{Cl+H_2(v=0),k_{\mathrm{trans}}(\omega),\Delta x}(x,y,t_0)$. In fact, $E_{\mathrm{tot}} = E_{H_2,v=1} + E_{\mathrm{x}}$ exceeds the potential barrier, $E_{\mathrm{tot}} > E^{\ddagger}$, and of course, it is larger than the reaction threshold; see marks $E_{\mathrm{d}} > E_{\mathrm{b}} > E_{\mathrm{a}}$ in Figure 3. For reasons of energy, one may, therefore, expect that the educts $Cl + H_2(v{=}1)$ induce the reaction → HCl + H (cf. eq 1); complementary aspects of the reaction dynamics will be discussed below. This "energetic" conjecture is verified by the subsequent snapshots of the wavepacket dynamics at $t = 95$ and 395 fs, shown in Figure 5b and c, respectively. Obviously, a substantial fraction of the wavepacket $\Psi_{Cl+H_2(v=1),k_{\mathrm{trans}}(\omega),\Delta x}(x,y,t)$ penetrates into the product domain $y > y_{\mathrm{b}}$ (see the lobe labeled B in Figure 5c), whereas the other parts are scattered back into the reactant valley of the PES (see the lobes labeled A_0 and A in Figure 5c). The corresponding reaction probability is $P_{Cl+H_2(v=1),E_{\mathrm{trans}}(\omega),\Delta x} = 0.6$; for comparison, the value for the IR + UV experiment is $P_{v=1}(\mathrm{IR{+}UV}) = 0.15$.[1] The relation $P_{v=1}(\mathrm{IR{+}UV}) = 0.15 < P_{Cl+H_2(v=1),E_{\mathrm{trans}}(\omega),\Delta x} = 0.6$ confirms the discussions of items (i) and (vii) in section IIA, that is, the present simple model provides an upper limit to the experimental reaction probabilities.

The nodal pattern of the lobe labeled A_0 reveals that it represents inelastic scatterings of the reactants $Cl + H_2(v = 1)$ to reactants $Cl + H_2(v' = 0)$. Likewise, the lobe labeled A is assigned tentatively to elastic scattering back to $Cl + H_2(v' = 1)$. A definite assignment of lobe A is prohibited, however, because a small fraction of $\Psi_{Cl+H_2(v=1),k_{\mathrm{trans}}(\omega),\Delta x}(x,y,t{=}395\ \mathrm{fs})$ is still in the interaction domain of the PES. Conservation of the total energy $E_{\mathrm{tot}} = E_{H_{2,v=1}} + E_{\mathrm{x}}$ implies that the lobe A_0 should move with much larger translational energy ($E'_{\mathrm{trans}} = E_{\mathrm{d}} = E_{\mathrm{tot}} - E_{H_2,v'=0}$) than lobe A ($E'_{\mathrm{trans}} = E_{\mathrm{x}} = E_{\mathrm{tot}} - E_{H_2,v'=1}$); compare labels E_{d} versus E_{x} in Figure 3. This conjecture is confirmed by the corresponding "movie" of the reaction dynamics, which consists of many sequential snapshots of $\Psi_{Cl+H_2(v=1),k_{\mathrm{trans}}(\omega),\Delta x}(x,y,t)$. They show that, indeed, the lobe labeled A_0 in Figure 5c returns back to the the reactant valley of the PES much faster than the lobe labeled A. Likewise, the lobe labeled B in the product domain is analyzed as a superposition of two partial waves representing products $HCl(v'{=}0) + H$ and $HCl(v'{=}1) + H$, as is obvious from the "meandering" interference pattern; at later times, these will branch into separate fast and slow partial waves for the products $HCl(v') + H$ with vibrational quantum numbers $v' = 0$ and 1, respectively. Apparently, the separation of the partial waves for

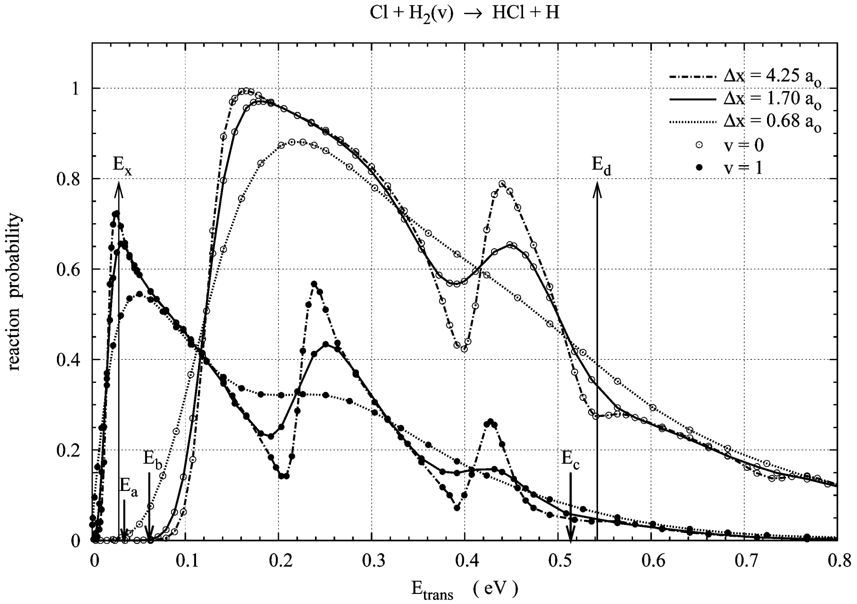

Figure 6. Reaction probabilies for the model Cl + $H_2(v{=}0) \rightarrow$ HCl + H (open symbols) and Cl + $H_2(\tilde{v}{=}1) \rightarrow$ HCl + H (black symbols) reactions in a *para*-H_2 crystal versus the translational energy E_{trans}. The initial wave functions are modeled as products of translational times vibrational wave functions (cf. eqs 40 and 41) but with arbitrary parameters for the momentum $k_{trans} = (2\mu_{Cl,H_2} \cdot E_{trans})^{1/2}/\hbar$ and for three representative values of the width Δx. The arrows mark the energies which have been labeled in Figure 3 as E_x, E_a, E_b, E_c, and E_d. The results for E_x, $\Delta x = 1.70$ a_0 and $v = 1$ versus $v = 0$ are related to the IR + UV versus “only UV” experiments of ref 1; see the text. Comparison of the results with the same total energy but different partitioning into vibrational plus translational energies, $E_{tot} = E_{H_2,v=1} + E_x$ (mark E_x) versus $E_{H_2,\tilde{v}=0} + \tilde{E}'_{trans}$ (mark E_d), reveals the dynamical effect which correlates with the Polanyi rules;[41,42] see the text.

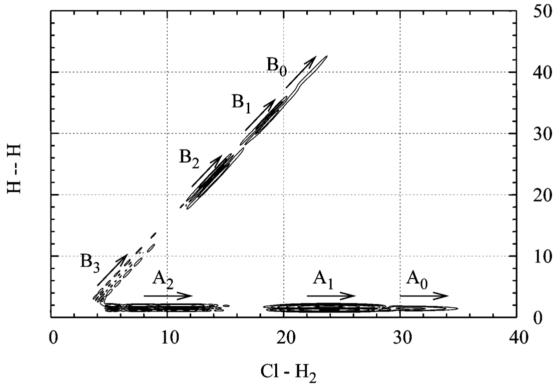

Figure 7. Same as Figure 5c but for the reactants Cl + $H_2(v{=}1)$ with the translational energy E_d. Snapshot taken at $t = 200$ fs.

the products is slower than that for the reactants. This is a consequence of the corresponding translational velocities, which scale as

$$v_{HCl+H,v'} = \hbar \cdot k_{HCl+H,v'}/\mu_{H,HCl} = \sqrt{\frac{2E'_{trans}}{\mu_{H,HCl}}} = \sqrt{\frac{2(E_{tot} - E_{HCl,v'})}{\mu_{H,HCl}}} \quad (55)$$

versus

$$v_{Cl+H_2,v'} = \sqrt{\frac{2(E_{tot} - E_{H_2,v'})}{\mu_{Cl,H_2}}} \quad (56)$$

where the ratio of the spacings between E_{tot} and the correponding vibrational energies is much smaller for the products than that for the reactants, respectively; compare Figure 3.

In order to investigate the role of the reaction dynamics, beyond the preceding energetic effects, we compare the wavepacket dynamics for reactants Cl + $H_2(v{=}1)$ and Cl + $H_2(\tilde{v}{=}0)$ with the same total energy but different partitionings into vibrational plus translational fractions, $E_{tot} = E_{H_2,v=1} + E_x = E_{H_2,\tilde{v}=0} + E_d$; compare eqs 3 and 4 and Figure 3. The corresponding translational momenta are $\hbar \cdot k_{trans} = (2\mu_{Cl,H_2}E_x)^{1/2}$ and $\hbar \cdot \tilde{k}_{trans} = (2\mu_{Cl,H_2}E_d)^{1/2}$, respectively, that is $\tilde{k}_{trans}$ is much larger than k_{trans}. The resulting snapshots are compared in Figure 5a−c (as discussed above) and 5d−f for $t = 0$, 50, and 240 fs, respectively. The density of the initial wave function $\Psi_{Cl+H_2(\tilde{v}=0),\tilde{k}_{trans},\Delta x}(x,y,t_0)$ (Figure 5d) is the same as that for $\Psi_{Cl+H_2(v=0),k_{trans}(\omega),\Delta x}(x,y,t_0)$ (Figure 4a), but the increase of the momentum from $k_{trans}(\omega)$ to $\tilde{k}_{trans}$ changes the nonreactivity of the slow wave function $\Psi_{Cl+H_2(v=0),k_{trans}(\omega),\Delta x}(x,y,t)$ (cf. Figure 4) into partial reactivity of the rapid $\Psi_{Cl+H_2(\tilde{v}=0),\tilde{k}_{trans},\Delta x}(x,y,t_0)$ (cf. Figure 5d,e). The reaction probability of $\Psi_{Cl+H_2(v=0),\tilde{k}_{trans},\Delta x}(x,y,t_0)$ is $P_{v=0,\tilde{E}_{trans},\Delta x} = 0.36$; this is just about half of the value $P_{v=0,E_{trans}(\omega),\Delta x} = 0.6$ for $\Psi_{Cl+H_2(v=0),k_{trans}(\omega),\Delta x}(x,y,t_0)$; compare Figure 5a−c. We conclude that the reaction probability is determined not only by the total energy E_{tot}, which is the same for both cases shown in Figure 5a−c and d−f, but also by the way that E_{tot} is partitioned into vibrational versus translational energies. The results documented in Figure 5 allow one to predict that the experimental IR + UV approach of ref 1, which puts most of the available energy E_{tot} into vibrational pre-excitation of $H_2(v{=}1)$ and only rather little into translational energy $E_{trans}(\omega) = E_x$, should be more efficient than a hypothetical (e.g., “only vacuum UV”?) experiment which would prepare the reactants with much higher translational energy $\tilde{E}_{trans}$ while keeping $H_2(\tilde{v}{=}0)$ in the vibrational ground state.

The results for the wavepacket dynamics documented in Figure 5a−c versus d−f can be rationalized in terms of the so-called Polanyi rules.[41,42] Accordingly, the reactivity is determined not only by the barrier height $E^{\ddagger}$ but also by its location. The energetic criterion suggests that, classically, the total energy E_{tot}

should exceed the potential barrier, $E_{tot} > E^{\ddagger}$, whereas quantum mechanically, tunneling through the barrier is possible even if E_{tot} is slightly below $E^{\ddagger}$. The dynamical criterion relates the location of the barrier to the efficiency of different partitionings of the total energy into vibrational plus translational fractions of the reactants, $E_{tot} = E_{vib} + E_{trans}$; the rules are applicable as long as E_{tot} is not all too much larger than $E^{\ddagger}$. For reference, Polanyi considered two limiting cases of "early" and "late" potential barriers, which are located in the reactant and product valleys of the PES $\tilde{V}(x_m,y)$, respectively (when plotted in mass-weighted coordinates x_m and y; cf. eq 50). The Polanyi rules predict that, in order to overcome those "early" or "late" barriers, the reactants need exclusively translational or vibrational energies, respectively. Now, the contour plot in Figure 2a of the present LEPS PES (and also the ab initio PES of Capecchi and Werner[17] to which it has been fitted) shows that its barrier is located neither "early" nor "late" but just in between, or "at high noon" (to generalize the illuminating terminology of J.C. Polanyi). As a working hypothesis, which is deduced by interpolation of Polanyi's two extreme cases, about equal shares of vibrational plus translational energies should be ideal to overcome the present "high noon" barrier. Since this ideal kind of equal partitioning of energy is impossible for the total energy E_{tot}, which is provided by the IR + UV experiment of ref 1, due to the vibrational quantization of the reactants, one is left with the second choice, that is, at least parts of the available energy should go into the two different vibrational and translational modes of the reactants. This "interpolated Polanyi rule for a high-noon barrier" allows one to explain the different quantum reaction dynamics, which is documented in panels a−c versus d−f of Figure 5, as follows. The scenario of Figure 5d−f invests the available energy of the reactants exclusively into translational energy, whereas the vibrational energy is restricted to zero-point energy. This entirely "nondemocratic" partitioning of the total energy should be less efficient than the case of Figure 5a−c, which provides nonzero (albeit not equal) fractions of energies into both degrees of freedom. Below, we shall add more details for the dynamical effects which underly the rather simple "interpolated Polanyi rule".

The phenomenon which has been noted for Figure 5c, that is, branching of the wavepacket into various slow versus fast partial waves for different high versus low vibrational excitations of the products and for corresponding scattering to the reactants, appears even more pronounced in Figure 5f. Specifically, the nodal patterns show that the separated lobes labeled A_0, A_1 and B_0, B_1 correspond to elastic and inelastic scattering into fast and slow reactants $Cl + H_2(v'=0)$ and $Cl + H_2(v'=1)$ and to fast and slow products $HCl(v'=0) + H$ and $HCl(v'=1) + H$, respectively.

The three examples for the wavepacket dynamics of the reactive and nonreactive reactions 1 and 2 (motivated by the IR + UV and "only UV" experiments of ref 1, respectively) and 3, which have been documented in Figures 5a−c, 4a−c, and 5d−f, respectively, will now serve as references for systematic investigations of the resulting reaction probabilities $P_{v,E_{trans},\Delta x}$. For this purpose, three sets of $P_{v=0,E_{trans},\Delta x}$ and $P_{v=1,E_{trans},\Delta x}$ for reactants $Cl + H_2(v=0)$ and $Cl + H_2(v=1)$, respectively, with three different values of the width parameter Δx are plotted versus translational energy E_{trans} in Figure 6. The case $\Delta x = 1.70\ a_0$ is close to the value listed in Table 2, for the limit of continuous-wave IR + UV coradiation ($\tau \rightarrow \infty$), that is, it is related to the IR + UV experiment of Anderson and co-workers.[1] Comparison with the other two cases, $\Delta x = 4.25\ a_0$ and $0.68\ a_0$, allows one to extrapolate the trends of the $Cl + H_2(v)$ reaction from quasi-infinite widths (as in molecular beam experiments in the gas phase) via the typical width in the *para*-H_2 quantum solid to quasi-zero-width; the latter corresponds to a hypothetical scenario of a "classical" H_2 solid where the centers of masses of the H_2 molecules are fixed to their equilibrium values in the solid. In the rather broad context of the results shown in Figure 6, the three examples which have been illustrated in Figures 5a−c, 4a−c, and 5d−f correspond to the mark E_x for the curve $P_{v=0,E_{trans},\Delta x=1.28a_0}$, mark E_x for $P_{v=1,E_{trans},\Delta x=1.28a_0}$, and mark E_d for $P_{v=0,E_{trans},\Delta x=1.28a_0}$, respectively.

Figure 6 reveals the following overall features of the reaction probabilities. All $P_{\nu,E_{trans},\Delta x}$ versus E_{trans} show rather steep increases, followed by modest falloffs at larger values of $E_{trans} < 0.8$ eV. The relevant consequences of these dominant trends for the interpretation of the experimental results of ref 1 will be discussed below; first, it is illuminating to consider the sawtooth-type signatures of resonances which are superimposed on the rise and falloffs of the $P_{\nu,E_{trans},\Delta x}$. These resonances correspond to Cl−H−H complexes with total energies and widths which are obvious from the sawtooth features of the $P_{v,E_{trans},\Delta x}$; for general discussions of these types of resonances, see, for example, refs 31, 38, and 44−46; suffice it here to say that the typical width of the resonances, $\Gamma_{res} \approx 0.05$ eV, corresponds to rather short lifetimes, $\tau_{res} = \hbar/\Gamma_{res} \approx 13$ fs. The amplitudes of the resonances increase with increasing widths Δx, approaching rather sharp resonance peaks in the limit $\Delta x \rightarrow \infty$, which corresponds to molecular beam experiments of the $Cl + H_2(v)$ reactions in the gas phase; the latter have been simulated by means of time-independent methods of scattering theory and analyzed first by Baer and co-workers.[14,15] Note that the complementary width of the momentum $\Delta k_{trans} = 0.5\hbar/\Delta x$ approaches zero as $\Delta x \rightarrow \infty$. Turning the table, decreasing values of the widths Δx imply increasing widths of the momenta Δk_{trans} and of the translational energies ΔE_{trans} (related to Δk_{trans} by $\Delta E_{trans}/E_{trans} \approx 2\Delta k_{trans}/k_{trans}$). As a consequence, decreasing values of Δx yield the reaction probabilities $P_{v,E_{trans},\Delta x}$, which correspond to a broader average of the neighboring values ($E_{trans} - \Delta E_{trans}/2 < E'_{trans} < E_{trans} + \Delta E_{trans}/2$) of the limit $P_{v=1,E_{trans},\Delta x\rightarrow\infty}$. In brief, they tend to "wash out" those sharp signatures of the reaction resonances in the gas phase. The results documented in Figure 6 show that, despite considerable "wash-out" effects due to the finite width Δx ($\approx 1.70\ a_0$) of the wave function representing the $Cl + H_2$ reaction (eq 1) in the quantum crystal *para*-H_2, (as compared to the gas phase), the features of reaction resonances in the $P_{v,E_{trans},\Delta x}$ are still significant. The curve $P_{v,E_{trans},\Delta x=0.68a_0}$ versus E_{trans} indicates that they should disappear completely for the hypothetical "classical" *para*-H_2 solid where $\Delta x \rightarrow 0$. This allows us to predict that modest signatures of reaction resonances, which were discovered first in the gas phase,[44] should also be observable for the $Cl + H_2(v)$ reaction in the quantum solid (but not for the hypothetical classical solid). In fact, close inspection of Figure 6 indicates that the value $P_{v=1,E_{trans},\Delta x=1.70a_0} = 0.65$ at $E_{trans} = E_x$ "profits" by a few percent from a resonance close to $E_{tot} = E_{H_2,v=1} + E_x$, whereas the smaller value $P_{v=0,E_{trans},\Delta x=1.70a_0}$ at $E_{trans} = E_d$ "suffers" by a few percent from the same resonance. Accordingly, the confirmation of the "interpolated Polanyi rule for a high-noon barrier", which has been discussed above, is still there, but it is actually less prominent if one subtracts the small effects of the resonances.

The "wash-out" effect due to decreasing values of the translational widths Δx which has been discovered for the resonances applies also to the phenomena at the reaction thresholds. Consider, for example, the sudden increase of

$P_{v=1,E_{\mathrm{trans}},\Delta x}$ versus E_{trans} close to the threshold $E_{\mathrm{tot}} = E_{\mathrm{H_2},v=1}$ (the case which supports reactivity according to the "interpolated Polanyi rule".) Close inspection of Figure 6 reveals that the rise of $P_{v=1,E_{\mathrm{trans}},\Delta x\rightarrow\infty}$ occurs close to $E_{\mathrm{trans}} = 0.01$ eV, that is, slightly above the threshold. The "wash-out" effect implies that the rise of $P_{v=1,E_{\mathrm{trans}},\Delta x=1.70\mathrm{a}_0}$ is less abrupt; it appears to increase with E_{trans} in a nearly linear manner from the very beginning. The corresponding "wash-out" effect for $P_{v=0,E_{\mathrm{trans}},\Delta x}$ at threshold appears to be even more pronounced than that for the case of $v = 1$. Figure 6 implies a rather steep rise of $P_{v=0,E_{\mathrm{trans}},\Delta x\rightarrow\infty}$ near $E_{\mathrm{trans}} = 0.12$ eV, that is well above the barrier. This "energetic delay" of the onset of the Cl + H_2(v=0) is in accord with the "interpolated Polanyi rule", that is, pure increase of translational energy in the domain $E_{\mathrm{HCl},v'=0} \leq E_{\mathrm{trans}} \lesssim 0.12$ eV is not efficient for climbing over the barrier of the PES. The "wash-out" effect at threshold implies that the rise of $P_{\nu=0,E_{\mathrm{trans}},\Delta x=1.70\mathrm{a}_0}$ versus E_{trans} starts at lower values of E_{trans}, compared to the sudden increase for $\Delta x \rightarrow \infty$; compare Figure 6. As a rather surprising consequence, the values of $P_{\nu=0,E_{\mathrm{trans}},\Delta x<\infty}$ are small but nonzero even for mean values E_{trans} of the translational energy below the threshold $E_{\mathrm{HCl},\nu'=0}$; for the present applications, $P_{\nu=0,E_{\mathrm{trans}}=E_{\mathrm{x}},\Delta x}$ are equal to 3.5×10^{-7} and 0.035 for $\Delta x =$ 1.70 and 0.68 a_0, respectively. These results suggests that the deviation of the experimental (= 0.006) value of the reaction probability from the ideal value, that is 0 below threshold, might also be due, in part, to the finite widths Δx of the representative wavepacket and to the related "wash-out" effect. Table 2 points to the origin of the finite widths Δx of the Cl + $H_2(\nu)$ reaction in the quantum solid: it is caused by the large width $\Delta R_{\mathrm{H_2}}$ of the broad distribution of the c.o.m. of the H_2 molecule in the Einstein cell representing the quantum crystal. As a consequence, it appears appropriate to consider the experimental observation of the small but nonzero reaction probability $P_{\nu=0}$("only UV") = 0.006 of the "only UV" experiment as a consequence of the quantum nature of the *para*-H_2 solid; the resulting "wash-out" effect would not occur in the gas phase; in the hypothetical limit of a classical solid where $\Delta x(\tau\rightarrow\infty,\Delta R_{\mathrm{Cl_2}}\rightarrow 0,\Delta R_{\mathrm{H_2}}\rightarrow 0) \rightarrow 0$ (compare eq 43) $P_{\nu=0}$("only UV") should have been much larger; compare Figure 6.

Having discussed the "wash-out" effects on the reaction resonances and on the rise phenomena of the $P_{v,E_{\mathrm{trans}},\Delta x}$ versus E_{trans} close to threshold, as a consequence of the broad widths $\Delta R_{\mathrm{H_2}}$ of the quantum solid, let us now turn to the overall smooth falloff of the $P_{v,E_{\mathrm{trans}},\Delta x}$ at larger translational energies E_{trans}. It may be explained in terms of a dynamical effect which is obvious from a comparison of the snapshots of the densities $\rho_{\mathrm{Cl+H_2}(v=1),k_{\mathrm{trans}}(\omega),\Delta x}(x,y,t)$ and $\rho_{\mathrm{Cl+H_2}(\tilde{v}=0),\tilde{k}_{\mathrm{trans}},\Delta x}(x,y,t)$ shown in Figure 5b and e, respectively. For reference, let us first consider the case of the small value of $E_{\mathrm{trans}}(\omega) = E_{\mathrm{x}}$, which is below the reaction barrier $E^{\ddagger}$. The corresponding Figure 5b reveals the dominant dynamical effect which induces reactivity of the Cl + H_2(v=1) reaction. The wave function hardly enters the "left corner" of the close interaction region of the PES; instead, this domain may be considered as a "dynamical white spot" on the landscape of the PES; compare with ref 47. Moreover, the wave function does not follow the reaction path via the barrier of the potential; this phenomenon has been investigated previously for different hydrogen-transfer reactions; see, for example, ref 50. Instead, it "cuts the corner", starting from the lobe of the reactant wave function which represents vibration of the pre-excited reactant molecule H_2(v=1) to its outer turning point, toward compressed configurations of the nascent product molecule HCl. This dynamical effect of the vibrational pre-excitation in the IR + UV experiment[1] is very efficient, causing the rise of the model reaction probability $P_{v=1,E_{\mathrm{trans}},\Delta x=1.70\mathrm{a}_0}$ versus E_{trans} to the maximum value close to 1.00; compare Figure 6. For comparison, the model reaction probability $P_{v=0,E_{\mathrm{trans}},\Delta x=1.70\mathrm{a}_0}$ for the UV-only experiment rises only to the maximum value close to 0.67.

In contrast with Figure 5b for the reference case of the small value $E_{\mathrm{trans}}(\omega) = E_{\mathrm{x}}$, Figure 5d shows that for a larger value of the translational energy $\tilde{E}_{\mathrm{trans}} = (\hbar\cdot\tilde{k}_{\mathrm{trans}})^2/(2\mu_{\mathrm{Cl,H_2}})$, the wavepacket penetrates into the strong interaction domain. Here, it climbs the steep repulsive wall of the PES in the "corner" of the interaction region, opposite to the reactant valley. From there, it is scattered back, partially to the opposite potential valley, with subsequent reflection (similar to the so-called relief reflections; cf. refs 48 and 49) such that the total wave function spreads out like a "double-headed dragon"; the reactive "head" of the wave function stretches out into the product valley of the PES, whereas the nonreactive "head" is repelled back to the reactant valley. Larger values of $\tilde{E}_{\mathrm{trans}}$ support that repulsion back to the reactant valley, at the expense of reactivity; this is the origin of the smooth falloff of $P_{v,E_{\mathrm{trans}},\Delta x}$ versus E_{trans} at larger vaules of $E_{\mathrm{trans}} \lesssim 0.8$ eV. The interfering motions of the "tail" and the "nonreactive head" of the wavepacket, presenting "penetration from the reactant valley into the corner of the interaction region" and "dominant repulsion from the steep wall of the PES back to the reactant valley", are obvious from the nodal patterns of $\rho_{\mathrm{Cl+H_2}(\tilde{v}=0),\tilde{k}_{\mathrm{trans}},\Delta x}(x,y,t)$ in the interaction region; compare Figure 5e.

Having discovered and explained the dynamical effects underlying the overall features of the reaction probabilities $P_{v,E_{\mathrm{trans}},\Delta x}$ versus E_{trans}, let us now re-examine, in view of those overall features, the example which has been motivated by the IR + UV experiments of ref 1, as shown in Figure 5a−c, and the case of Figure 5d−f which has been investigated in order to discover the effects of quantum dynamics, beyond the pure energetic effects. Previously, we have introduced the "interpolated Polanyi rule for the high-noon potential barrier" of the Cl + H_2 reaction in order to explain the enhanced reactivity of the Cl + H_2(v=1) reaction 1 compared to the Cl + H_2($\tilde{v}$=0) reaction 3, for the same total energy E_{tot}, eq 4. The preceding analysis allows us to discover important additional details of the quantum dynamics. On one hand, the corresponding mark E_{x} for $P_{v=1,E_{\mathrm{trans}}(\omega)=E_{\mathrm{x}},\Delta x=1.70\mathrm{a}_0} = 0.67$ shows that this is close to the maximum of the curve $P_{v=1,E_{\mathrm{trans}},\Delta x=1.70\mathrm{a}_0}$ versus E_{trans}, that is, the rather small value of E_{x} which is induced by UV photodissociation of the Cl_2 precursor in the quantum solid H_2, combined with the vibrational pre-exciation of the H_2(v=1) reactant molecule, turns out as the rather ideal case supporting the (relative) maximum of reactivity, which is even slightly supported by a reaction resonance. The favorable, rather small value of $E_{\mathrm{trans}}(\omega) = E_{\mathrm{x}}$ is a consequence of the experimental UV frequency, combined with the kinematic effect of the Cl + H_2 reaction in the quantum solid, which depends on the atomic masses of the reactants; compare eq 45. A hypothetical scenario which would convert a larger fraction of the kinetic energy ΔE of the photodissociated chlorine atoms into translational energy for reaction would cause a counterintuitive effect, that is, it would not support but diminish the reactivity of the Cl + H_2(v=1) reaction in the quantum solid. On the other hand, we recognize that the mark E_{d} for $P_{\tilde{v}=0,\tilde{E}_{\mathrm{trans}}=E_{\mathrm{d}},\Delta x=1.70\mathrm{a}_0} = 0.34$ does not sit on the maximum of $P_{v=0,\tilde{E}_{\mathrm{trans}},\Delta x=1.70\mathrm{a}_0}$ but far in the falloff domain due to the rather larger value of the translational energy $\tilde{E}_{\mathrm{trans}} = E_{\mathrm{d}} = E_{\tilde{v}=0} + E_{\mathrm{x}}$. Obviously, sitting in the falloff domain is less favorable than being on top; hence, the partitioning of the total reactant energy into $E_{H_2,v=1} + E_{trans}$ is more favorable than $E_{H_2,\tilde{v}=0} + \tilde{E}_{trans}$.

An extreme consequence of the "falloff" behavior of the $P_{v,E_{trans},\Delta x}$ versus E_{trans} is the case of $v = 1$, $E_{trans} = E_d$ documented in Figure 6; see mark E_d for the curve $P_{v=1,E_{trans},\Delta x=1.70a_0}$. Even though the total energy $E_{tot} = E_{v=1} + E_d$ is almost twice the value for the case of $v = 1$, $E_{trans} = E_x$, the reaction probability has dropped from 0.67 to 0.047 in the falloff domain. In addition, Figure 7 also documents the branching of the wavepacket $\Psi_{Cl+H_2(v=1),\tilde{k}_{trans},\Delta x}(x,y,t)$ into various lobes, similar to the results documented in Figure 5c and f. Specifically, the lobes labeled A_0, A_1, and A_2 correspond to inelastic and elastic scatterings into reactants $Cl + H_2(v'=0)$, $Cl + H_2(v'=1)$, and $Cl + H_2(v'=2)$ with rapid, medium, and slow velocities, respectively. Likewise, lobes B_0, B_1, and B_2 correspond to products $HCl(v'=0) + H$, $HCl(v'=1) + H$, and $HCl(v'=2) + H$ with rapid, medium, and slow velocities, respectively. The assignment of the lobe labeled B_3 is not definite as part of it is still residing in the interaction domain. Most likely, it is bound to evolve to ultraslow products $HCl(v'=3) + H$.

These rather rich effects of the quantum dynamics of the $Cl + H_2(v=1)$ reaction in solid *para*-H_2 contribute to the overall result, which has been summarized above as the "interpolated Polanyi rule". In particular, we could show that the apparent "second choice" criterion of that extended Polanyi rule actually corresponds to rather optimal partitioning of the total energy E_{tot} into large and small fractions of vibrational versus translational energies of the reactants, respectively, yielding (relative) optimal reactivity of the IR + UV experiment of ref 1.

IV. Conclusions

The IR + UV versus "only UV" experiments of the group of D. T. Anderson[1] have motivated the present, first quantum model simulation of a state-selective chemical reaction in a quantum solid, specifically, reactions 1−4 for reactants $Cl + H_2(v=1)$ versus $Cl+H_2(\tilde{v}=0)$ in a *para*-H_2 crystal. Our model is based on the assumptions and approximations which have been discusssed in section IIA and below. Hence, it is obvious that the present work must be considered only as a first step into a rich field—the quantum theory for chemical reactions in quantum solids. The results which have been derived using the present model must be considered, therefore, as preliminary. Nevertheless, it may serve as a reference for more realistic models. We hope that they will stimulate more sophisticated theoretical and experimental investigations. With this caveat, we summarize below some of the results which have been presented and discussed in section III, in particular, those which we consider as important in view of the experiments of ref 1.

(a) The experimental parameters which would allow control of the processes, eqs 1, 2, and possibly 3 subject to the condition of eq 4, include the frequency ω of the UV laser for photodissociation of the precursor molecule Cl_2 embedded in the *para*-H_2 crystal. It may be used, in principle, to excite Cl_2 in selective electronic excited states that produce the atomic reactants Cl in different electronic states and with different translational energies E_{trans}. The kinetics of the reaction with the given small mass ratio m_H/m_{Cl} imply, however, that only a rather small fraction (on the order of m_H/m_{Cl}) of the kinetic energy of the photodissociated Cl atoms is converted into translational energy E_{trans} of the reactants, whereas the "rest" is "wasted" as energy of the c.o.m. of the reactive system relative to the solid; compare eq 45. As a consequence, the range of the values E_{trans} which can be controlled by means of the laser frequency ω is restricted to rather small values. In the context of the present model, the recent work by Wang et al.[21] is quite stimulating as it suggests that the overall reactivity of the $Cl + H_2$ reaction may be enhanced for excited atoms $Cl(^2P_{1/2})$ and small translational energies of the reactants, an obvious challenge to the experimentalists!

(b) Another parameter that one may consider for control of the reaction is the duration τ of the laser pulse. It influences the translational widths Δx of the wave function representing the reactants. This is a very important parameter, in principle; for example, it allows one to compare, or distinguish, the results for the reaction in the quantum solid with, or from, the limits of the gas phase ($\Delta x \rightarrow \infty$ for $\tau \rightarrow \infty$) and the hypothetical case of a "classical" H_2 solid ($\Delta x \rightarrow 0$). However, again, the variations of Δx depending on the experimental parameter τ are rather limited, close to the value which is imposed by the width $\Delta R_{H_2} = 1.21\ a_0$ of the motion of the c.o.m. of the H_2 molecules in Einstein-type cells of the *para*-H_2 crystal[22] (cf. Table 2 and eq 43) with the mass factor $c_1 = m_{Cl}/(m_{Cl} + 2m_H) \approx 1$ for the term depending on ΔR_{H_2}. This constraint on Δx is a special effect of the quantum solid. An advantage is that the theoretical results are quite robust with respect to the pulse duration τ. This allowed us to employ convenient, rather short pulse durations ($\tau = 5-50$ fs) for the quantum dynamics simulations in order to extrapolate the results for the long, quasi-continuous wave pulses which are used in the IR + UV experiment.[1]

(c) The much larger reactivity of the IR + UV experiment causing reaction 1, compared to the "only UV" experiment causing preferably elastic scattering (reaction 2), has been explained as a consequence of energetic plus dynamical effects. The energetic effect is rather simple, that is, for the "only UV" experiment, the mean value of the total energy for the system Cl−H−H consists only of the small value of translational energy, eq 45, which is below threshold and below the reaction barrier height (see labels $E_x < E_a < E_b$ in Figures 3 and 6). In contrast, the IR + UV experiment supplies additional vibrational energy such that the total energy is well above the threshold and the potential barrier (see labels $E_d > E_b > E_a$ in Figures 3 and 6). The quantitative results for the reaction probability depend, however, not only on the total energy but also on the specific partitioning into fractions of translational plus vibrational energy.

(d) A variety of dynamical effects have been discovered by the quantum dynamics simulations, which contribute to the experimental results. Several of these (for the details, see section III) may be summarized by the "interpolated Polanyi rule", which interpolates between two limiting cases of the original Polanyi rules, that is, the requirements of exclusively translational or vibrational energies of the reactants, in order to overcome "early" and "late" potential barriers which are located in the reactant and product valleys of the PES, respectively.[41,42] We employ a LEPS PES which has been fitted to the ab initio PES of Capecchi and Werner,[17] where the barrier is neither "early" nor "late" but at "high noon" between the reactant and product valleys, similar to the empirical LEPS PES of Baer.[14] For this case, the "interpolated Polanyi rule" requires specific partitionings of the total energy into adequate fractions of translational plus vibrational energies; for various other extensions of the original Polanyi rules, see, for example, refs 51 and 52. Systematic investigations reveal that the special conditions of the IR + UV experiment correspond to the most efficient partitioning into rather large plus small fractions of vibrational plus translational energies, respectively, causing an (relative) optimum of reactivity. This very favorable experimental partitioning of energy must perhaps be considered as incidental; it is a challenge to test similar scenarios for other reactions in quantum solids, for example, $Br + H_2(v) \rightarrow HBr + H$ in *para*-H_2 or $Cl + D_2(v) \rightarrow DCl + D$ in *ortho*-D_2.

(e) We have discovered two effects of the quantum solid which contribute to the experimental results of ref 1. Both are due to the characteristic, rather broad distribution of the c.o.m. of the H_2 molecules in the corresponding Einstein cell representing the *para*-H_2 crystal, $\Delta R_{H_2} = 1.21$ a_0.[22] The corresponding finite widths of the representative wavepackets of the reactants (see item (b)) are associated with corresponding widths of the translational momenta and energies. In the quantum solid, these tend to average or "wash-out" two features of the reaction probabilities versus the translational energies, compared to the gas phase. First, at specific energies, the reaction may proceed via more or less short-lived so-called reaction resonances in the gas phase.[31,38,44] These are associated with peak-type features of the reaction probabilities versus translational energy. We predict that these types of resonances should also be observable in the quantum solid, albeit with reduced structures of the resonance peaks due to the "wash-out" effect. In fact, we predict that the favorable reactivity observed in the IR + UV experiment[1] profits from reaction resonances of the $Cl + H_2(v=1)$ reaction close to threshold, even though, quantitatively, this is a rather small effect (few percent). Second, the "wash-out" effect supports a modest amount of reactivity even when the mean values of the total energy are below the reaction thershold. It is very possible that this effect contributes to the observed small reactivity of the "only UV" experiment.

We anticipate that extended investigations, beyond the assumptions and approximations of the present simple model will allow discovery of additional effects of the quantum solid on the elementary reactions 1−4 or similar reactions. Work along these lines is in progress.

Acknowledgment. This paper is dedicated to Prof. R. Benny Gerber (Jerusalem) on the occasion of his 65th birthday, with gratitude for very pleasant, fruitful, and stimulating cooperation in the field of photoinduced ultrafast molecular processes in matrixes over many years. We would like to express our sincere thanks to Professor D. T. Anderson (Laramie) for stimulating discussions and for providing his experimental results (ref 1, experimental tandem paper) prior to publication and to A. Accardi (Berlin), Prof. O. Kühn (Rostock) and to Prof. N. Schwentner (Berlin) and his group, also for stimulating discussions. Financial support by the Deutsche Forschungsgemeinschaft (Project Sfb 450 TP C1) and continuous support by Fonds der Chemischen Industrie is also gratefully acknowledged.

References and Notes

(1) Kettwich, S. C.; Raston, P. L.; Anderson, D. T. *J. Phys. Chem. A* **2009**, *113*, 10.1021/jp811206a.

(2) Raston, P. L.; Anderson, D. T. *Phys. Chem. Chem. Phys.* **2006**, *8*, 3124.

(3) Yoshioka, K.; Raston, P. L.; Anderson, D. T. *Int. Rev. Phys. Chem.* **2006**, *25*, 469.

(4) Fajardo, M. E.; Tam, S.; DeRose, M. E. *J. Mol. Struct.* **2004**, *695*, 111.

(5) Yoshioka, K.; Anderson, D. T. *J. Chem. Phys.* **2003**, *119*, 4731.

(6) Momose, T.; Fushitani, M.; Hoshina, H. *Int. Rev. Phys. Chem.* **2005**, *24*, 533.

(7) Lundell, J.; Cohen, A.; Gerber, R. B. *J. Phys. Chem. A* **2002**, *106*, 11950.

(8) Khriachtchev, L.; Tanskanen, H.; Lundell, J.; Pettersson, M.; Kiljunen, H.; Räsänen, M. *J. Am. Chem. Soc.* **2003**, *125*, 4696.

(9) Feldman, V. I.; Sukhov, F. F.; Orlov, A. Y.; Tyulpina, I. V. *J. Am. Chem. Soc.* **2003**, *125*, 4698.

(10) Khriachtchev, L.; Tanskanen, H.; Cohen, A.; Gerber, R. B.; Lundell, J.; Pettersson, M.; Kiljunen, H.; Räsänen, M. *J. Am. Chem. Soc.* **2003**, *125*, 6876.

(11) Khriachtchev, L.; Isokoski, K.; Cohen, A.; Räsänen, M.; Gerber, R. B. *J. Am. Chem. Soc.* **2008**, *130*, 6114.

(12) Gerber, R. B. *Annu. Rev. Phys. Chem.* **2004**, *55*, 55.

(13) Persky, A.; Klein, F. S. *J. Chem. Phys.* **1966**, *44*, 3617.

(14) Baer, M. *Mol. Phys.* **1974**, *27*, 1429.

(15) Persky, A.; Baer, M. *J. Chem. Phys.* **1974**, *60*, 133.

(16) Skouteris, D.; Manolopuolos, D. E.; Bian, W.; Werner, H.-J.; Lai, L.-H.; Liu, K. *Science* **1999**, *286*, 1713.

(17) Capecchi, G.; Werner, H. J. *Chem. Phys. Phys. Chem.* **2004**, *6*, 4975.

(18) Skouteris, D.; Laganà, A.; Capecchi, G.; Werner, H.-J. *Int. J. Quantum Chem.* **2004**, *99*, 577.

(19) Balucani, N.; Skouteris, D.; Capozza, G.; Segoloni, E.; Casavecchia, P.; Alexander, M. H.; Capecchi, G.; Werner, H.-J. *Phys. Chem. Chem. Phys.* **2004**, *6*, 5007.

(20) Mahapatra, S. *Int. Rev. Phys. Chem.* **2004**, *23*, 483.

(21) Wang, X.; Dong, W.; Xiao, C.; Che, L.; Ren, Z.; Dai, D.; Wang, X.; Casavecchia, P.; Yang, X.; Jiang, B.; Xie, D.; Sun, Z.; Lee, S.-Y.; Zhang, D. H.; Werner, H.-J.; Alexander, M. H. *Science* **2008**, *322*, 573.

(22) Kühn, O.; Manz, J.; Schild, A. In preparation.

(23) Silvera, I. F. *Rev. Mod. Phys.* **1980**, *52*, 393.

(24) Operetto, F.; Pederiva, F. *Phys. Rev. B* **2006**, *73*, 184124.

(25) Korolkov, M. V.; Manz, J. *Z. Phys. Chem.* **2003**, *217*, 115.

(26) Alekseyev, A. B.; Korolkov, M. V.; Kühn, O.; Manz, J.; Schröder, M. *J. Photochem. Photobiol. A: Chem.* **2006**, *180*, 262.

(27) Korolkov, M. V.; Manz, J. In *Analysis and Control of Ultrafast Photoinduced Reactions*; Kühn, O., Wöste, L., Eds.; Springer Series in Chemical Physics; Springer-Verlag, Berlin, 2007; Vol. 87, Chapter 4.10, p 352.

(28) London, F. *Z. Elektrochem.* **1929**, *35*, 552.

(29) Eyring, H.; Polanyi, M. *Z. Phys. Chem. B* **1931**, *12*, 279.

(30) Sato, S. *J. Chem. Phys.* **1955**, *23*, 592.

(31) Henriksen, N. E.; Hansen, F. Y. *Theories of Molecular Reaction Dynamics*; Oxford University Press: Oxford, U.K., 2008.

(32) Kokh, D. B.; Alekseyev, A. B.; Buenker, R. J. *J. Chem. Phys.* **2001**, *115*, 9298.

(33) Kokh, D. B.; Alekseyev, A. B.; Buenker, R. J. *J. Chem. Phys.* **2004**, *120*, 11549.

(34) Connor, J. N. L.; Jakubetz, W.; Manz, J. *Mol. Phys.* **1978**, *35*, 1301.

(35) Connor, J. N. L.; Jakubetz, W.; Manz, J.; Whitehead, J. C. *J. Chem. Phys.* **1980**, *72*, 6209.

(36) Bargheer, M.; Cohen, A.; Gerber, R. B.; Gühr, M.; Korolkov, M. V.; Manz, J.; Niv, M. Y.; Schröder, M.; Schwentner, N. *J. Phys. Chem. A* **2007**, *222*, 9573.

(37) Marston, C. C.; Balint-Kurti, G. G. *J. Chem. Phys.* **1981**, *91*, 3571.

(38) Tannor, D. J. *Introduction to Quantum Mechanics: A Time-Dependent Perspective*; University Science Books: Sausalito, CA, 2007; Vol. 111, p 9573.

(39) Apkarian, V. A.; Schwentner, N. *Chem. Rev.* **1999**, *99*, 1481.

(40) Korolkov, M. V.; Manz, J. *Chem. Phys. Lett.* **2004**, *393*, 44.

(41) Polanyi, J. C. *Acc. Chem. Res.* **1972**, *5*, 161.

(42) Polanyi, J. C. *Science* **1987**, *236*, 680.

(43) Neuhauser, D. *Chem. Phys. Lett.* **1992**, *200*, 173.

(44) Lee, Y. T. *Angew. Chem., Int. Ed. Engl.* **1987**, *26*, 939.

(45) Bisseling, R. H.; Kosloff, R.; Manz, J.; Mrugała, F.; Römelt, J.; Weichselbaumer, G. *J. Chem. Phys.* **1987**, *86*, 2626.

(46) Bisseling, R. H.; Gertitschke, P. L.; Kosloff, R.; Manz, J. *J. Chem. Phys.* **1989**, *88*, 6191.

(47) Gertitschke, P. L.; Kiprof, P.; Manz, J. *J. Chem. Phys.* **1987**, *87*, 941.

(48) Gerber, R. B.; Korolkov, M. V.; Manz, P.; Niv, M. Y.; Schmidt, B. *Chem. Phys. Lett.* **2000**, *327*, 76.

(49) Chaban, G.; Gerber, R. B.; Korolkov, M. V.; Manz, J.; Niv, M. Y.; Schmidt, B. *J. Phys. Chem. A* **2001**, *105*, 2770.

(50) Hartke, B.; Manz, J. *J. Am. Chem. Soc.* **1988**, *110*, 3063.

(51) Daniel, C.; Heitz, M.-C.; Lehr, L.; Manz, J.; Schröder, T. *J. Phys. Chem.* **1993**, *97*, 12485.

(52) Daniel, C.; de Vivie-Riedle, R.; Heitz, M.-C.; Manz, J.; Saalfrank, P. *Int. J. Quantum Chem.* **1996**, *57*, 595.

JP9003455